Investigating drivers of particulate matter pollution over India and the implications for radiative forcing with GEOS-Chem-TOMAS15

Alexandra Karambelas[1], Arlene M. Fiore[1], Daniel M. Westervelt[1], V. Faye McNeill[2], Cynthia A. Randles[3], Chandra Venkataraman[4], Jeffrey R. Pierce[5], Kelsey R. Bilsback[5], and George P. Milly[1]

[1]Lamont-Doherty Earth Observatory Columbia University
[2]Chemical and Environmental Engineering Columbia University
[3]ExxonMobil Technology and Engineering Company
[4]Department of Chemical Engineering Indian Institute of Technology Bombay
[5]Department of Atmospheric Science Colorado State University

November 24, 2022

Abstract

Ambient fine particulate matter (PM2.5) concentrations in India frequently exceed 100 μg/m3 during fall and winter pollution episodes. We use the GEOS-Chem chemical transport model with the TwO-Moment Aerosol Sectional microphysics scheme with 15 size bins (TOMAS15) to assess PM2.5 composition and impacts on radiation and cloud condensation nuclei (CCN) during pollution episodes as compared to the seasonal (October-December) average. We conduct high resolution (0.25 degree x0.3125 degree) nested-domain simulations over India for short-duration, high-PM2.5 episodes in fall 2015 and 2017. The simulations capture the magnitude and spatial patterns of pollution episodes measured by surface monitors (r2PM2.5=0.69) although aerosol optical depth is underestimated. During the episodes, near-surface organic matter (OM), black carbon (BC), and secondary inorganic aerosol concentrations increase from seasonal averages by up to 36, 7, and 7 μg/m3, respectively. Episodic aerosol increases enhance cooling by lowering the top-of-atmosphere clear-sky direct radiative effect (DRETOA) during the 2015 episode (-6 W/m2), with a smaller impact during the 2017 episode (-1 W/m2). Differences in DRETOA reflect larger increases in scattering aerosols in the column during the 2015 episode (+17 mg/m2) than in 2017 (+13 mg/m2), while absorbing aerosol column enhancements are smaller (+3 mg/m2) in both years. Changes in shortwave radiation at the surface (SWsfc) are spatially similar to DRETOA and mostly negative during both episodes. CCN enhancements during these episodes occur across the western Indo-Gangetic Plain, coincident with higher PM2.5 concentrations. Changes in DRETOA, SWsfc, and CCN during high-PM2.5 episodes may have implications for crops, the hydrologic cycle, and surface temperature.

Investigating drivers of particulate matter pollution over India and the implications for radiative forcing with GEOS-Chem-TOMAS15

Alexandra Karambelas[1,*], Arlene M. Fiore[1,2,^], Daniel M. Westervelt[1,7], V. Faye McNeill[3], Cynthia A. Randles[4], Chandra Venkataraman[5], Jeffrey R. Pierce[6], Kelsey R. Bilsback[6], George P. Milly[1]

[1] Lamont-Doherty Earth Observatory, Columbia University, Palisades, NY USA
* Now at Northeast States for Coordinated Air Use Management, Boston, MA USA
[2] Department of Earth and Environmental Sciences, Columbia University, New York, NY USA
^Now at Department of Earth, Atmospheric and Planetary Sciences, Massachusetts Institute of Technology, Cambridge, MA, USA
[3] Chemical and Environmental Engineering, Columbia University, New York, NY USA
[4] ExxonMobil Technology and Engineering Company, Annandale, NJ USA
[5] Department of Chemical Engineering, Indian Institute of Technology Bombay, Mumbai, India
[6] Department of Atmospheric Science, Colorado State University, Fort Collins, CO USA
[7] NASA Goddard Institute for Space Studies, New York, NY, USA

Corresponding Author: Alexandra Karambelas (akarambelas@nescaum.org)

Key Points:

- We establish a new high-resolution India domain nested within a global chemistry model with an option for detailed aerosol microphysics
- $PM_{2.5}$ pollution episodes over India vary spatially but are commonly dominated by carbonaceous aerosols.
- Increased scattering aerosols during episodes lower top-of-atmosphere direct radiative effect, enhance cooling and reduce surface shortwave

Abstract

Ambient fine particulate matter ($PM_{2.5}$) concentrations in India frequently exceed 100 μg/m^3 during fall and winter pollution episodes. We use the GEOS-Chem chemical transport model with the TwO-Moment Aerosol Sectional microphysics scheme with 15 size bins (TOMAS15) to assess $PM_{2.5}$ composition and impacts on radiation and cloud condensation nuclei (CCN) during pollution episodes as compared to the seasonal (October-December) average. We conduct high resolution (0.25°x0.3125°) nested-domain simulations over India for short-duration, high-$PM_{2.5}$ episodes in fall 2015 and 2017. The simulations capture the magnitude and spatial patterns of pollution episodes measured by surface monitors ($r^2_{PM2.5}$=0.69) although aerosol optical depth is underestimated. During the episodes, near-surface organic matter (OM), black carbon (BC), and secondary inorganic aerosol concentrations increase from seasonal averages by up to 36, 7, and 7 μg/m^3, respectively. Episodic aerosol increases enhance cooling by lowering the top-of-atmosphere clear-sky direct radiative effect (DRE_{TOA}) during the 2015 episode (-6 W/m^2), with a smaller impact during the 2017 episode (-1 W/m^2). Differences in DRE_{TOA} reflect larger increases in scattering aerosols in the column during the 2015 episode (+17 mg/m^2) than in 2017 (+13 mg/m^2), while absorbing aerosol column enhancements are smaller (+3 mg/m^2) in both years. Changes in shortwave radiation at the surface (SW_{sfc}) are spatially similar to DRE_{TOA} and mostly negative during both episodes. CCN enhancements during these episodes occur across the western Indo-Gangetic Plain, coincident with higher $PM_{2.5}$ concentrations. Changes in DRE_{TOA}, SW_{sfc}, and CCN during high-$PM_{2.5}$ episodes may have implications for crops, the hydrologic cycle, and surface temperature.

1. Introduction

In recent decades, ambient air pollution in India has grown increasingly worse alongside population growth, economic development, urbanization, and motorization with limited implementation or enforcement of regulations on air pollutant emissions. One such pollutant, fine particulate matter with diameters smaller than 2.5 micrometers ($PM_{2.5}$), regularly exceeds India's National Ambient Air Quality Standard (NAAQS) of 40 μg/m^3 for annual mean $PM_{2.5}$. Fifty-eight percent of districts exhibit $PM_{2.5}$ concentrations greater than the India NAAQS (Chowdhury et al., 2019), and up to 99.9% of the population lives in areas exceeding the World Health Organization (WHO) annual mean guideline of 10 μg/m^3. Anthropogenic source sectors contribute approximately 60% of India's annual average population-weighted $PM_{2.5}$ concentrations (Venkataraman et al., 2018).

In addition to its role in air pollution, PM (also referred to as aerosols) affects climate by altering the energy balance of the planet through its interactions with radiation and clouds. In this way, aerosols exert a radiative forcing (IPCC, 2013) on climate, which can lead to disruptions in the monsoon (Dave et al., 2017; Westervelt et al., 2020) and agriculture (Burney & Ramanathan, 2014; Gupta et al., 2017). The climate impacts from PM depend on composition, size (diameter), and mass, and are thus expected to vary in space and time as the balance of PM sources, and their overall magnitude, change. For example, strong seasonal variations in concentrations and composition will affect bulk optical properties as the mix of black carbon (BC; strongly absorbing) and sulfate (strongly scattering) varies (Bellouin et al., 2016). Aerosols can affect or modify the direct radiative effect (DRE)—the difference in instantaneous net (downward - upward) radiative flux at the top of the atmosphere (TOA) induced by the presence of aerosol. For instance, TOA direct radiative effects of aerosols from the waste combustion sector alone range from -0.3 to -0.05 W/m^2 over India (Kodros et al., 2016). Aerosols also impact regional and global climate indirectly through cloud processes (Albrecht, 1989; Twomey, 1977; Rosenfeld et al., 2008), also known as aerosol indirect effects, which are among the biggest uncertainties in projecting future climate change (Myhre et al., 2013).

Major anthropogenic sources of PM in India include residential biomass (Conibear et al., 2018; Venkataraman et al., 2018), coal-fired power plants (Guttikunda & Jawahar, 2014), waste burning (Kodros et al., 2016), and anthropogenic dust (Philip et al., 2017), each of which produces a different chemical mix

of both particulate, or primary PM, and gaseous emissions leading to secondary PM. For instance, satellite instruments have detected a 50% increase of sulfur dioxide, a byproduct of coal-fired power plants and precursor gas to sulfate aerosol, between 2007 and 2017 (C. Li et al., 2017). Particulate pollution in India exhibits an annual cycle, with highest surface concentrations in winter associated with a shallow planetary boundary layer and less precipitation and lowest during the monsoon season because of rainout. $PM_{2.5}$ concentrations during fall and wintertime pollution episodes have been recorded in the several hundreds and even approaching 1000 $\mu g/m^3$. Episodic contributors to local and regional $PM_{2.5}$ pollution include sources such as seasonal agricultural burning (Liu et al., 2018), the national Diwali holiday (Gautam et al., 2018), and natural sources like windblown dust. Venkataraman and co-authors (2018) find the biggest contributions from agricultural burning (approximately 18%) are in the states where the emissions occur—Punjab and Haryana—and also directly downwind in Delhi. Additionally, enhanced aerosol may be present at different times throughout the year, for instance windblown dust from nearby deserts in March through May or persistent Indian outflow over the Bay of Bengal year-round (David et al., 2018). With $PM_{2.5}$ concentrations projected to increase in the future due to higher emissions of organic matter and secondary inorganic aerosols, and enhanced windblown dust under climate change (Pommier et al., 2017; Venkataraman et al., 2018), it is increasingly important to understand the current PM composition of scattering and absorbing aerosols for quantifying future changes and their resulting climate implications.

Although sectoral impacts to air quality at present and under future scenarios have been investigated in India (Chowdhury et al., 2018; Schnell et al., 2018; Venkataraman et al., 2018), less attention has been given to episodic pollution events in India, with almost no focus on a compositional analysis, or the implications for climate. For example, although wintertime haze events in urban China are largely composed of secondary aerosols (Huang et al., 2015), including elevated concentrations during the COVID-19 related shutdowns across China (Huang et al., 2020; Shi & Brasseur, 2020), the extent to which these findings are transferable to urban India is unclear.

Using the GEOS-Chem global model with a nested high-resolution regional simulation over India, we examine changes in $PM_{2.5}$ aerosol microphysics and the associated direct radiative effect (DRE) during 5-day peak pollution episodes in fall 2015 and 2017 compared to the annual average (2015) and seasonal average environment (2015 and 2017); an additional episode from 2016 is included in the Supplemental Information. We use a high-resolution (0.25° x 0.3125°) nested grid over India with the TwO-Moment Aerosol Sectional (TOMAS) aerosol microphysics package (Adams & Seinfeld, 2002; Kodros & Pierce, 2017; Ramnarine et al., 2019) to simulate PM mass and number size distributions, and chemical composition. We identify variations in PM composition during peak pollution episodes relative to seasonal and annual mean values. We compare the baseline model simulations with the limited available *in situ* observations and satellite aerosol optical depth. Finally, with an offline radiative transfer code that prescribes optical properties based on the PM composition and size bins for TOMAS as simulated in GEOS-Chem, we assess the aerosol DRE at TOA during seasonal average and episodic pollution levels. We also evaluate changes in aerosol number and cloud condensation nuclei (CCN) as a proxy for the impacts of PM on clouds, an indirect climate impact of aerosols. Our findings suggest peak PM pollution episodes alter local DRE at TOA by up to -6 W/m^2 and enhance CCN by up to 280%.

2. Model description and simulation methodology

2.1 Air Quality Modeling

We use the GEOS-Chem chemical transport model version 12.0.2 (https://doi.org/10.5281/zenodo.1455215) with standard tropospheric chemistry (Bey et al., 2001), with and without TOMAS aerosol microphysics. We run simulations both at a global 2° x 2.5° domain and using a newly developed nested domain over India from 0-40 °N and 60-100 °E at 0.25° x 0.3125° (161 by 162 grid cells). This domain also includes Afghanistan, Bangladesh, Bhutan, Nepal, Pakistan, and parts

of neighboring countries. This domain was loosely based on prior work at a 0. 5° x 0.667° resolution with MERRA-2 meteorological fields from Chaliyakunnel et al. (2019). Stratospheric ozone chemistry is calculated via the Linoz module (McLinden et al., 2000). We use the baseline tropospheric chemistry (NO_X-O_X-HC-aerosol-Br) with the simple secondary organic aerosol scheme (Pai et al., 2020). We use the global ECLIPSE anthropogenic emission inventory for year 2015 (Stohl et al., 2015) processed through the Harvard-NASA Emissions Component (HEMCO) (Keller et al., 2014). Landscape fire emissions, including agricultural fires, for 2015, 2016, and 2017 are from the Global Fire Emissions Database (GFED, https://www.globalfiredata.org) with small fires and seasonal fire count and emissions updates in the states of Punjab and Haryana (Liu et al., 2019). During the simulation, GFED emissions are updated at a 3-hourly timescale, and ECLIPSE emissions are scaled monthly from annual total emissions. Meteorology is from GEOS-FP for 2015-2017 (Lucchesi, 2013). We processed global GEOS-FP fields from the 0.25° x 0.3125° global dataset for the nested domain.

TOMAS15 simulates prognostic aerosol number and mass size distributions for 7 chemical species (sulfate, sea salt, dust, hydrophilic and hydrophobic elemental and organic carbon, and aerosol water), with 15 sections spanning 3 nm to 10 μm in diameter. Particulate pollutant contributions to total $PM_{2.5}$ are simulated by GEOS-Chem with TOMAS15, hereafter GC-TOMAS15, for sulfate, sea salt, BC, organic matter (OM), and dust, while nitrate and ammonium are from the standard GEOS-Chem "Tropchem," hereafter GC-Tropchem. Sulfate concentrations in the bulk scheme will not necessarily match those in the TOMAS scheme, particularly as aerosol plumes are transported away from sources as the representations of dry and wet deposition differ in the size-resolved and bulk aerosol schemes. Our use of bulk ammonium and nitrate distributed across TOMAS size sections may not be consistent with thermodynamic equilibrium calculations. However, this technique is a compromise between completely neglecting nitrate in TOMAS versus including a computationally intensive online treatment of size-dependent ammonium nitrate partitioning. Average contributions from sea salt and dust during episodes are typically very low in the model across India (< 3%), which is expected considering these episodes fall outside peak windblown dust seasons, thus we do not include sea salt and dust in our analysis. We quantify modeled aerosol component contributions at the surface and in the total column to seasonal and episodic mean concentrations. We calculate seasonal and episodic CCN using aerosol number concentration from GC-TOMAS15 and Kappa-Kohler theory (Petters & Kreidenweis, 2007). We note that clouds are not directly modified by aerosols in our simulations as they are prescribed in the model from the GEOS-FP analysis. An advantage that TOMAS15 provides over the GEOS-Chem bulk aerosol model is the more physically realistic size-dependent calculation of AOD and related aerosol optical properties. One disadvantage is that anthropogenic fugitive dust is not included, which may be a large seasonal contributor to $PM_{2.5}$ in India; this dataset is included in the standard GC-Tropchem model simulations (Philip et al., 2017), but to our knowledge the size distribution has not been evaluated, so fugitive dust is not included in the size-resolved TOMAS simulations.

We conduct one baseline standard tropospheric chemistry simulation without TOMAS15 (i.e. using Tropchem) globally at coarse horizontal resolution (2° x 2.5°) for the years 2014-2017 to establish boundary conditions, where 2014 is solely for initialization purposes. We additionally conduct a full year baseline Tropchem simulation for 2015 with the regional model (0.25° x 0.3125° horizontal resolution) over India. Due to the computational cost of enabling GC-TOMAS15, we simulate 2014-2015 globally at coarse resolution (2° x 2.5°)—again discarding 2014 as initialization—with subsequent global simulations restricted to August-December for 2016 and 2017 when PM episodes are highest over India, where August and September are for initialization only. The 2016 and 2017 GC-TOMAS runs are initialized with August 2015 restart files to reduce spin-up time. We rely on these coarse resolution global simulations for our assessment of climate impacts quantified with the radiative transfer model as we evaluate changes during episodic enhancements relative to seasonal means.

With the GC-TOMAS15 high-resolution regional model, we conduct a series of 5-day simulations (plus a 5-day initialization period from the coarse resolution output) corresponding to peak episodes in $PM_{2.5}$ observed at the U.S. Embassy in Delhi: December 5-9 2015, November 1-5 2016, and November 6-10 2017 (Supplemental Figure 1). These episodes are purposely selected to be outside of the Diwali holiday each year, which occurs annually between mid-October and mid-November, as those emissions are not included in the emissions inventory, though the event contributes to air pollution (e.g. Mukherjee et al., 2020). Daily-average anthropogenic organic carbon (OC) emissions are similar between the 2015 October-December average, 2015 episode, and 2017 episode; biomass burning emissions are nearly double the 2015 seasonal average during the 2017 episode but are roughly half during the 2015 episode (Supplemental Figure 2). Because the 2016 and 2017 episodes are similar in aerosol distribution and climate impacts, we compare the December 2015 and November 2017 episodes in the main text and provide a similar analysis of 2016 in the Supplemental Information. Episodes are compared to the October-December seasonal average from their respective year. We evaluate spatial changes in air pollutant abundances, $PM_{2.5}$ composition, and metrics for local climate impacts across the Indo-Gangetic Plain as well as the entire sub-continent during the peak pollution events in Delhi compared to seasonal averages.

Model aerosol optical depth (AOD) is calculated offline using GC-TOMAS output and the radiative transfer code described below following Kodros et al., (2016), and includes black and organic carbon, sulfate, nitrate, ammonium, dust, aerosol water, and sea salt. For AOD observations, we use the Dark Target Level 3 (L3 collection 6) atmosphere daily product retrieved from the Moderate Resolution Imaging Spectroradiometer (MODIS) instrument aboard the Terra and Aqua satellites. This 1° x 1° gridded product is obtained via NASA's Giovanni data portal. The Dark Target MODIS retrieval compares better than Deep Blue versus both the ground-based AERONET AOD over South Asia and the higher-resolution MAIAC retrieval (see Figure 8 of Mhawish et al., 2019).

2.2 Radiative transfer model

We use the Rapid Radiative Transfer Model for Global Climate Models (RRTMG) offline and adapted for use with GEOS-Chem TOMAS by Colorado State University (Bilsback et al., 2020a; Bilsback et al., 2020b). Briefly, we use RRTMG to estimate the DRE, or the instantaneous radiative impact at TOA due to episodic aerosol enhancement under clear sky conditions relative to the seasonal average during the selected $PM_{2.5}$ pollution episodes, using our 2° x 2.5° GC-TOMAS15 simulations (as we only have the 5-day episodes available from the high-resolution GC-TOMAS15 simulations). We use November solar parameters and three-year GEOS-FP modeled meteorological conditions seasonal averages for the 2015-2017 October-December time frame. We only change the aerosol fields ingested by RRTMG, which include hydrophilic and hydrophobic BC, organic carbon, sulfate, nitrate, ammonium, dust, sea salt, and aerosol water during the specified time period (i.e., episode or seasonal). Note that aerosol water was calculated in all GEOS-Chem simulations according to time-varying relative humidity in the GEOS-FP input meteorology. We also evaluate the change in solar radiation reaching the surface, which has implications for crop growth and the hydrologic cycle.

In calculating DRE, we consider two limiting aerosol mixing states: either fully external or core-shell internal. If external, organic carbon and BC form separate spherical particles. If internal, a BC core is surrounded by other species in a homogenously mixed shell (Jacobson, 2001). Our DRE estimates thus provides bounds, where core-shell internal mixing serves as a warmer (more positive) forcing and the external mixture a cooler (more negative) forcing. Aerosol number concentration and size distributions are equal across both mixing states. We calculate the change in DRE during the episode from the seasonal mean as:

$$\Delta DRE_{TOA} = (SW_{TOA\ down} - SW_{TOA\ up})_{episode} - (SW_{TOA\ down} - SW_{TOA\ up})_{seasonal\ mean} \quad (1)$$

such that DRE_{TOA} is a negative quantity for both episode and seasonal mean. Since $SW_{TOA\ down}$ does not change between episode and seasonal mean in RRTMG, this equation in effect translates to the change in SW reflected upwards, such that a decrease in DRE_{TOA} indicates an increase in SW reflected upwards during the episode (i.e. a relative radiative cooling impact). For calculating the change in SW at the surface, the parallel equation is:

$$\Delta SW_{sfc} = (SW_{sfc\ down} - SW_{sfc\ up})_{episode} - (SW_{sfc\ down} - SW_{sfc\ up})_{seasonal\ mean} \quad (2)$$

3. Evaluating modeled $PM_{2.5}$ concentrations

We evaluate the baseline simulations with annual and episodic average *in situ* observations of total $PM_{2.5}$ from the Central Pollution Control Board (CPCB) in India as well as satellite observations of aerosol optical depth (AOD) in the visible wavelength (~550 nm). Observations of $PM_{2.5}$ are sparse in India, and for the December 5-9, 2015 episode, we find 18 sites with hourly observations available for model evaluation located in northern and central India. Data were collected via the CPCB web portal (https://app.cpcbccr.com/ccr/#/caaqm-dashboard-all/caaqm-landing/data). The average high-resolution modeled $PM_{2.5}$ concentrations for the December 5-9, 2015 episode from the baseline nested India Tropchem (Figure 1a) simulation are on average 28% lower than from GC-TOMAS15 (Figure 1b). Distributions between GC-Tropchem and GC-TOMAS are not expected to be identical for inorganic aerosol, BC, and OM even if emissions were all the same because of size-dependent atmospheric chemistry, wet removal, and dry deposition relative to the bulk aerosol scheme (Supplemental Figure 3). Spatial correlations between episode average simulated and all available observed concentrations are strong (Table 1; $r^2_{Tropchem\ high\text{-}res}$=0.69 and $r^2_{TOMAS15\ high\text{-}res}$=0.67), suggesting that both model configurations capture spatial $PM_{2.5}$ concentration gradients across India. At all available monitoring locations, average observed $PM_{2.5}$ concentrations during the pollution episode are 142 μg/m^3; high-resolution GC-TOMAS15 episode average concentrations are 125 μg/m^3 and GC-Tropchem concentrations are lower at 95 μg/m^3. At measurement sites that exhibited elevated $PM_{2.5}$ during the time period (e.g. change in episodic $PM_{2.5}$ from seasonal average > 0), the average observed concentration was 190 μg/m^3 or 34% higher than the nationwide observed average. Average modeled concentrations are lower than observed during this time period, and neither GC-TOMAS (excess average at monitors 84 μg/m^3 or +4% higher than episodic average) nor GC-Tropchem (67 μg/m^3 or +5%) at the coarse resolution can fully replicate these excess concentrations. Chemical transport models are known to underestimate peak fine $PM_{2.5}$ events in Asia (e.g. Wang et al., 2014), and both coarse resolution model configurations are biased low against annual average observations (at monitor locations by up to 62 μg/m^3, Supplemental Figure 4 and Supplemental Table 1). All evaluation metrics (spatial correlations, temporal correlations, and biases against observations) improve during periods of pollution episodes like in December 2015 at both coarse- and high- resolution simulations (Table 1; Supplemental Table 1). As expected, higher resolution simulations produce a wider range in concentrations, as well as larger enhancements in $PM_{2.5}$ during the episode relative to the seasonal average (Supplemental Figure 5). Although each model configuration has its own set of strengths and weaknesses as discussed above, we find that overall the high-resolution simulations with TOMAS fall closest to the observations during the high-pollution episodes on which we focus our study.

Retrievals of AOD from MODIS suggest the nested GC-TOMAS15 underestimates total column AOD during the pollution events when modeled concentrations are highest (Figure 2; MODIS measurements aboard Aqua are similar to those from Terra and are shown along with comparisons for the November 2016 episode in Supplemental Figure 6). Modeled AOD, sampled at satellite overpass time, is biased low for both episodes, during which the model simulates only about 60% of the MODIS AOD, reflecting an

unknown combination of underestimated column burdens (including aerosol water uptake) and/or poorly represented optical properties. Model AOD shows some skill over east India and Bangladesh compared to satellite retrievals during the 2015 episode, which may be related to aerosol composition during this particular episode as discussed below.

While the simulated AOD here is significantly lower than the MODIS Dark Target product, David et al. (2018) have previously shown that during the months in which our episodes occur, their modeled AOD falls between the much lower MISR product and the L2 Collection 6 MODIS product which uses the Deep Blue retrieval over land and the Dark Target retrieval over oceans. Mhawish et al. (2019), however, show that the Deep Blue retrieval underestimates the AOD retrieved from AERONET and from the higher resolution MAIAC product retrieved from MODIS over South Asia. Hence, there is uncertainty in the observed AOD as well as in the model. Finally, some of our low model bias may be attributable to the lack of emissions of anthropogenic fugitive dust (Philip et al., 2017) or domestic waste burning including trash (Wiedinmyer et al., 2014) in GC-TOMAS15, which contribute considerably to annual total PM emissions, although the extent to which these sectors contribute to pollution episodes is unknown. The AOD (and surface $PM_{2.5}$) could be further improved in TOMAS15 by the incorporation of size-resolved sources of anthropogenic fugitive dust (Philip et al., 2017; Xia et al., 2022) and domestic trash (and other waste) burning (Wiedinmyer et al., 2014), though an overestimate in wet removal resulting from excessive light rain (Wang et al. 2021) could explain the common underestimate in both GEOS-Chem configurations that we use here. Mindful of these model biases, we turn next to examine the influence of episodic enhancements on aerosol concentration and composition and direct and indirect climate impacts.

4. Surface $PM_{2.5}$ and compositional changes during peak pollution episodes

During the December 5-9 2015 episode, $PM_{2.5}$ concentrations in the high-resolution domain average 36 $\mu g/m^3$ nationwide but exceed 190 $\mu g/m^3$ in Delhi and in the eastern states of Bihar and West Bengal (Figure 3a). By subtracting episodic total $PM_{2.5}$ or component contributions from the seasonal average using the global coarse resolution configuration with which we simulate the seasonal average, it is possible to quantify the "excess" $PM_{2.5}$ during the pollution episodes. Regions of positive $PM_{2.5}$ enhancement are separated from negative changes by the green contours in Figures 3, 4, 6, and 7. Excess $PM_{2.5}$ in the December 2015 episode is centered over the eastern IGP where concentration enhancements compared to the 2015 October-to-December mean exceed 50 $\mu g/m^3$ (Figure 3b). For comparison, the episodic average concentration from the coarse GC-TOMAS simulation is also shown (Figure 3c). Episodic concentrations increase by 15% on average in India, with increases up to 30% in eastern India. Some decreases of 4-6 $\mu g/m^3$ occur over western India. Episodic contributions of BC, OM, and the combined sulfate, nitrate, and ammonium (hereafter referred to as secondary inorganics) follow a similar spatial distribution as the total concentration enhancement from the seasonal average, with elevated concentrations over Northwest India, Delhi, and across the eastern IGP. During the 2015 episode, OM is the component with the largest absolute enhancements, with large swaths of 10-15 $\mu g/m^3$ excess OM across the IGP (Figure 3e). Enhancements are smaller for BC (<4 $\mu g/m^3$ Figure 3d). Secondary inorganics increase by 5-7 $\mu g/m^3$, but these enhancements are more localized to eastern India (Figure 3f) than for the carbonaceous aerosols.

During the November 6-10 2017 episode, $PM_{2.5}$ concentrations average 32 $\mu g/m^3$ nationwide but reach 171 $\mu g/m^3$ in Delhi, with elevated concentrations stretching across the IGP (Figure 4a), similar to the 2015 episode. $PM_{2.5}$ concentration enhancements during the 2017 episode from the October-December 2017 seasonal average, however, are largest in northwest India over Punjab, Delhi, and into western Uttar Pradesh (Figure 4b), with enhancements generally between 10 and 30 $\mu g/m^3$ and a maximum enhancement of 52 $\mu g/m^3$. Decreases of 5-20 $\mu g/m^3$ relative to the seasonal average occur over eastern and central India during the 2017 episode, in contrast to the 2015 episode (compare Figures 3b and 4b). During the 2017 episode, changes in BC concentrations relative to the October to December average are small, between -

2 μg/m^3 and +6 μg/m^3 (Figure 4d). Changes in OM are larger, with decreases in the eastern IGP of 9 μg/m^3 and increases in the western IGP up to 36 μg/m^3 (Figure 4e). Secondary inorganic aerosol broadly decreases by 4-6 μg/m^3 from the seasonal average across much of eastern India during the episode, but increases over western Uttar Pradesh, Delhi, Punjab, and Haryana by up to 6 μg/m^3 (Figure 4f). The November 1-5 2016 episode shows similar spatial distributions in episodic average total $PM_{2.5}$ and enhancement of $PM_{2.5}$ and components as the 2017 episode (Supplemental Figure 7).

Our model analysis indicates that these three pollution episodes in India are driven by increases in BC, OM, and secondary inorganic aerosols, with OM contributing the largest changes (Figures 3 and 4, Supplemental Figure 7). In regions of positive $PM_{2.5}$ enhancements from the October to December seasonal mean, the episodic changes in these three $PM_{2.5}$ components relative to the seasonal mean vary. At the surface during the 2015 episode, OM, BC, and secondary inorganic aerosols increase on average by 4.7 μg/m^3, 1.2 μg/m^3, and 1.1 μg/m^3, respectively. The average magnitude increases in these components during the 2017 episode are similar (+6.0 μg/m^3 for OM, +1.4 μg/m^3 for BC, +0.8 μg/m^3 for secondary inorganic aerosols).

5. Implications of pollution episodes for local energy balances

Aloft, there are major differences between the 2015 and 2017 episode, especially above the boundary layer (Figure 5). During the 2015 episode, BC, OM, and secondary inorganic concentrations increase above the boundary layer by 200-300% from the seasonal average, while during the 2017 episode there are more moderate increases of 50-100% in the mid-troposphere and a corresponding increase in secondary inorganic aerosols by up to 60% in the lower troposphere (Figure 5). The vertical profile of aerosols in the 2016 episode shows a lower overall enhancement and similar distribution to the 2017 episode (Supplemental Figure 8).

Total column enhancements from the October to December seasonal average for BC, OM, and secondary inorganic aerosol show spatial similarities to the surface $PM_{2.5}$ enhancements for the 2015 episode (compare Figure 6a-c with Figure 3). Strong, isolated column increases of BC (Figure 6a), OM (Figure 6b), and secondary inorganic aerosols (Figure 6c) occur over eastern India and Bangladesh, while the OM enhancements are larger in magnitude (> 30 mg/m^2) and relatively more widespread. Using aerosol fields archived from GC-TOMAS15, we calculate the change in clear-sky DRE for both external (Figures 6d; 7d) and core-shell (Supplemental Figure 9) mixing assumptions with the offline RRTMG model and find little quantitative difference in DRE or surface shortwave (<1 W/m^2) between these two bounding assumptions. During the December 5-9 2015 episode, enhanced aerosol scattering leads to a 6 W/m^2 decrease in DRE_{TOA} over the eastern states of Bihar, Jharkhand, and West Bengal, and over Bangladesh (Figure 6d). A negative sign in DRE at TOA indicates a relative cooling tendency and more shortwave radiation reflected out of the atmosphere by aerosols during the episode as compared to seasonal mean conditions. Similarly, there is a widespread reduction in the amount of shortwave (SW) radiation (up to 15 W/m^2) reaching the surface (Figure 6e).

During the November 6-10, 2017 episode, aerosol column burden enhancements occur over northwestern India including the states of Punjab and Haryana, Delhi, and western Uttar Pradesh (Figure 7a-c). Over this region, the OM aerosol burden enhancement compared to seasonal average is between 20 and 30 mg/m^2 (Figure 7b), while BC (Figure 7a) and secondary inorganic aerosol (Figure 7c) enhancements are less than 10 mg/m^2. Despite increased aerosol concentrations over northwest India, DRE_{TOA} decreases by only 0.5-1.5 W/m^2 on average in this region (Figure 7d). During the 2017 episode, DRE_{TOA} increases up to 2 W/m^2 over southern and eastern India compared to the October to December average, indicating a decrease in backscattered radiation that aligns spatially with the decrease in scattering aerosol (OM and

secondary inorganic). Surface SW exhibits broad decreases of up to 9 W/m^2 over much of northwestern India and strong increases of over 4 W/m^2 where there is decreased aerosol at the surface (Figure 7e).

Changes in the contributions of each component to the column aerosol enhancement vary spatially by episode and by altitude. Despite similar surface-level magnitude enhancements in regions where peak levels of aerosols occur during the two episodes, the changes in DRE_{TOA} differ, reflecting different column burden changes and vertical distributions (Figure 5). We investigate the cause of this difference by comparing the enhancements in scattering (the sum of secondary inorganics and OM) and absorbing (BC) aerosols over the regions where the column aerosol burden is enhanced (Figures 6a-c and 7a-c). During both episodes, BC column burdens increases on average by about +3 mg m^{-2}, but scattering aerosols increase more during the 2015 episode (+17 mg m^{-2}) than in 2017 (+13 mg m^{-2}), with notable differences in the vertical distribution of the changes between the two episodes shown in Figure 5. More scattering aerosol mass in the 2015 episode reflects more SW than in the 2017 episode, leading to a larger change in DRE_{TOA} in 2015 than 2017. The scattering aerosol column burden enhancement is even smaller during 2016 (+9 mg m^{-2}) than in either 2015 or 2017, leading to small changes in DRE_{TOA} relative to the seasonal average (Supplemental Figure 10, up to +2 W/m^2). Aerosol mass changes of OM and BC in the regions where they change are approximately the same between the 2015 and 2017 episodes, suggesting that the differences in DRE_{TOA} between the two episodes may be due to the different magnitude and directional changes in sulfate.

Finally, we examine changes in cloud condensation nuclei (CCN) concentrations to gauge cloud changes due to aerosol-cloud interactions. Enhancement in episode average CCN (0.2% supersaturation) is most concentrated over the states of Punjab and Haryana and into Delhi and western Uttar Pradesh, with a column episodic enhancement of over 800 CCN cm^{-2} compared to the October to December average, with a slightly lower yet still elevated CCN concentration across the IGP for all three pollution episodes (Figures 6f; 7f; Supplemental 10f). The CCN enhancements are co-located with elevated surface $PM_{2.5}$ during episodes (compare Figures 6f, 7f with Figures 3b, 4b) and total aerosol particle number (Supplemental Figure 11). Although not an exact match, enhanced CCN column burdens often coincide spatially with increases in surface aerosol concentration more than with column burdens. In regions of $PM_{2.5}$ enhancement from the respective year seasonal average, India-total aerosol mass increases of fine mode (less than 1μm) OM, BC, and secondary inorganic aerosols are +15%, +24%, and +9% for the 2015 episode and +17%, +22%, and -3% for the 2017 episode. Total (including supermicron sizes) OM, BC, and secondary inorganic aerosol mass increases from respective seasonal averages are +19%, +27%, and +12%, respectively, for the 2015 episode and +19%, +24%, and -2% for the 2017 episode. Increases in aerosol number and CCN over the western IGP during both episodes may be related to stagnant conditions conducive to pollution accumulation. Changes in meteorology from the 2015 seasonal mean during the pollution episodes include shallower planetary boundary layers coincident with regions of excess $PM_{2.5}$ during the episodes (Supplemental Figure 12), which could reflect local feedbacks between aerosols and atmospheric stability (Z. Li et al., 2017; Slater et al., 2022; Wilcox et al., 2016). Cloud cover increases during the 2015 episode, although decreases occur during the 2016 and 2017 episodes (Supplemental Figure 12). Wind speeds do not vary significantly between seasonal average and episode, and there is no clear pattern in relative humidity (not shown).

6. Summary and Discussion

In this study, we use two regional and two global configurations of the GEOS-Chem model to determine changes in total $PM_{2.5}$ mass and composition and the response of climate-relevant metrics (direct radiative effect, CCN, surface shortwave radiation) during peak pollution episodes relative to the overall October to December pollution season over India. Our newly established regional configuration simulates a high resolution (0.25° x 0.3125°) domain over India with boundary conditions from the global coarse resolution

(2° x 2.5°) GEOS-Chem model. A major advance for evaluating climate metrics such as aerosol-radiation and aerosol-cloud interactions is the use of the TOMAS aerosol microphysics scheme, which enables an evaluation of aerosol mass and size distributed across 15 size bins. We simulate air quality using the standard tropospheric chemistry GEOS-Chem platform (Tropchem) as well as the TOMAS 15-bin aerosol microphysics scheme (GC-TOMAS15) for the first time with the high-resolution nested India domain for 5-day long enhanced $PM_{2.5}$ episodes in December 2015 and November 2017 that were identified using observations at the U.S. Embassy in Delhi (November 2016 episode in the Supplemental Information). We find that episodic $PM_{2.5}$ mass concentrations are on average 15% greater than seasonal average concentrations across the IGP in India, with localized maximum concentration changes upwards of 100% compared to seasonal average, and reflect combined enhancements in BC, OM, and secondary inorganics. The absolute changes in OM are larger than the changes in BC and secondary inorganic aerosols, with little to no contributions from dust and sea salt.

We use an offline radiative transfer model (RRTMG) to calculate changes in clear-sky DRE_{TOA} and SW_{sfc} during two pollution episodes relative to seasonal mean conditions (October to December). Where aerosols increase during a pollution episode, clear-sky DRE_{TOA} is generally negative, implying an overall cooling influence from the aerosol enhancements. In the December 5-9, 2015 episode, reductions (more negative) in DRE_{TOA} (up to -6 W/m^2) and in SW_{sfc} (up to -15 W/m^2) radiation coincide spatially with enhancements in scattering aerosols (secondary inorganics and OM) and absorbing aerosols (BC) both at the surface and in the column. Conversely, during the November 6-10, 2017 episode, changes to DRE_{TOA} are only minimally negative, coincident with increased aerosols (up to -1 W/m^2) compared to the seasonal average, yet there are substantial reductions in SW_{sfc} (up to -7 W/m^2). We find that the change in clear-sky DRE_{TOA} from the October to December average depends on the relative change in scattering versus absorbing aerosol components. Here we find that there is a larger relative increase in scattering aerosol column burden during the 2015 episode leading to a stronger negative DRE_{TOA}, while scattering aerosols decline slightly in the 2017 episode and lead to virtually no change in DRE_{TOA}. Our findings suggest that aerosol and local climate influences are likely to vary with the particular characteristics of a pollution episode. As expressed in Xia et al. (2022) we expect feedbacks on local meteorology such as suppressed planetary boundary layer height, which would continue to exacerbate pollution. We also expect the simulated pollution events to worsen with the addition of missing inventories such as anthropogenic fugitive dust and trash burning. Additionally, we use aerosol number concentration from TOMAS and Kappa-Kohler theory to estimate changes in CCN, an indicator of aerosol indirect effect, as a proxy for episodic impacts on clouds. CCN enhancements are highly concentrated over Delhi during both episodes and coincident with enhanced inorganic aerosol concentrations during the 2015 episode. Regions of high CCN resulting from pollution episodes may subsequently influence radiative forcing and cloud cover, suppressing precipitation (smaller cloud droplets; reduced surface evaporation) and vertical mixing (less surface shortwave reduces buoyancy), however we did not directly model these feedbacks.

From the modeled surface concentrations and contributions, we infer that increased concentrations at the U.S. embassy in Delhi may signal a broader geographical pollution episode, affecting the length of the IGP. The pan-Indian pollution problem has been documented previously using air quality models (Karambelas et al., 2018) and satellite products (Ravishankara et al., 2020). Modeled concentrations in $PM_{2.5}$ pollution "hot spots" top 100 $\mu g/m^3$, although the regions of greatest relative enhancements differ between episodes, likely reflecting different causes of the pollution episodes. For example, the 2015 wintertime episode may have been triggered by synoptic meteorology favorable for the stagnation of anthropogenic pollution, while the 2016 and 2017 episodes may be more strongly influenced by seasonal agricultural fires (e.g. Roozitalab et al., 2020). Aerosol composition is critical to revealing climate impacts, and the GC-TOMAS15 platform aims to support this understanding. Limitations of this work include comparing episodes to seasonal average at coarse resolution due to computational constraints, and

neglecting brown carbon in the offline radiative transfer code. Further work is needed to understand source contributions to BC, OM, and secondary organics and the extent to which our findings may generalize more broadly to other pollution episodes over northern India.

Data Availability Statement

Data and code including GEOS-Chem model output, HEMCO diagnostic output, and RRTMG output calculated by this project and presented in figures and tables are hosted on the Columbia University Academic Commons at (URL TBD) (Karambelas et al., 2022).

Acknowledgements

We acknowledge ExxonMobil Research and Engineering Company for supporting this work. The GEOS-FP data used in this study/project have been provided by the Global Modeling and Assimilation Office (GMAO) at NASA Goddard Space Flight Center. We acknowledge Dr. Gus Correa for help with data archival.

Figure Captions

Figure 1 Average $PM_{2.5}$ concentrations during the December 5-9 2015 episode simulated with the regionally nested high-resolution GEOS-Chem model over India for a) Tropchem and b) GC-TOMAS15 overlaid with observations from the CPCB. The values in the lower left indicate the model area average (in $\mu g/m^3$) and full range within India

Table 1 Model evaluation of $PM_{2.5}$ with all available CPCB observations in India averaged over the October-November-December season or during the December 5-9 2015 pollution episode as shown in parentheses. Correlations are spatial.

Figure 2. AOD from MODIS Aqua (left column; Dark Target retrieval algorithm) compared with GC-TOMAS15 1:30 PM local time averaged for each pollution episode (right column) during December 5-9 2015 (top row) and November 6-10 2017 (bottom row).

Figure 3 a) Average December 5-9 2015 episode $PM_{2.5}$ concentration (0.25 x 0.3125 GC-TOMAS15); and concentration enhancements during the episode relative to seasonal average for (all 2 x 2.5) b) $PM_{2.5}$ c) average December 5-9 2015 episode $PM_{2.5}$ concentrations in the 2 x 2x.5 simulation d) black carbon (BC) e) organic matter (OM); f) the sum of inorganic aerosols (sulfate, nitrate, and ammonium). A single contour denoting zero change in total $PM_{2.5}$ is superimposed in green.

Figure 4 Same as Figure 3 except for the November 6-10 2017 episode.

Figure 5 Average concentration differences in the column above regions where the surface $PM_{2.5}$ episodic enhancement is positive, for (a) black carbon, (b) organic matter, and (c) secondary inorganic aerosol. The red lines are for the relative (%) change of the 2017 episode from the 2017 October to December average and blue shows the relative (%) change of the 2015 episode from the 2015 October to December average.

Figure 6 Changes in the column burdens of a) black carbon b) organic matter c) secondary inorganics during the December 5-9, 2015 pollution episode from seasonal average (October-December) in the GC-TOMAS15 coarse horizontal resolution (global) simulations (seasonal fields are only available at coarse resolution). Also shown are changes during the episode from the seasonal mean of d) direct radiative effect (DRE) at the top of the atmosphere (TOA); e) net surface shortwave (SW) radiation; f) total column cloud

condensation nuclei (0.2% supersaturation). The singular contour for zero change is shown in green. Negative DRE and SW are indicative of cooling.

Figure 7 Same as Figure 6 except for the November 6-10, 2017 episode.

References

Adams, P. J., & Seinfeld, J. H. (2002). Predicting global aerosol size distributions in general circulation models. *Journal of Geophysical Research*, *107*(D19). https://doi.org/10.1029/2001JD001010

Albrecht. (1989). Aerosols, Cloud Microphysics, and Fractional Cloudiness. Science, 245(4923), 3131227–1230. https://doi.org/10.1126/science.245.4923.1227

Bellouin, Nicolas, Baker, L., Hodnebrog, Ø., Olivié, D., Cherian, R., Macintosh, C., et al. (2016). Regional and seasonal radiative forcing by perturbations to aerosol and ozone precursor emissions. *Atmospheric Chemistry and Physics*, *16*(21), 13885–13910. https://doi.org/10.5194/acp-16-13885-2016

Bey, I., Jacob, D. J., Yantosca, R. M., Logan, J. A., Field, B. D., Fiore, A. M., et al. (2001). Global modeling of tropospheric chemistry with assimilated meteorology: Model description and evaluation. *Journal of Geophysical Research: Atmospheres*, *106*(D19), 23073–23095. https://doi.org/10.1029/2001JD000807

Bilsback, K. R., Kerry, D., Croft, B., Ford, B., Jathar, S. H., Carter, E., et al. (2020). Beyond SO_x reductions from shipping: assessing the impact of NO_x and carbonaceous-particle controls on human health and climate. *Environmental Research Letters*, *15*(12), 124046. https://doi.org/10.1088/1748-9326/abc718

Bilsback, K. R., Baumgartner, J., Cheeseman, M., Ford, B., Kodros, J. K., Li, X., et al. (2020). Estimated Aerosol Health and Radiative Effects of the Residential Coal Ban in the Beijing-Tianjin-Hebei Region of China. *Aerosol and Air Quality Research*, *20*(11), 2332–2346. https://doi.org/10.4209/aaqr.2019.11.0565

Burney, J., & Ramanathan, V. (2014). Recent climate and air pollution impacts on Indian agriculture. *Proceedings of the National Academy of Sciences*, *111*(46), 16319–16324. https://doi.org/10.1073/pnas.1317275111

547 Chaliyakunnel, S., Millet, D. B., & Chen, X. (2019). Constraining Emissions of Volatile Organic
548 Compounds Over the Indian Subcontinent Using Space-Based Formaldehyde Measurements.
549 *Journal of Geophysical Research: Atmospheres*, *124*(19), 10525–10545.
550 https://doi.org/10.1029/2019JD031262
551 Chowdhury, S., Dey, S., & Smith, K. R. (2018). Ambient PM2.5 exposure and expected premature
552 mortality to 2100 in India under climate change scenarios. *Nature Communications*, *9*(1).
553 https://doi.org/10.1038/s41467-017-02755-y
554 Chowdhury, S., Dey, S., Guttikunda, S., Pillarisetti, A., Smith, K. R., & Di Girolamo, L. (2019). Indian
555 annual ambient air quality standard is achievable by completely mitigating emissions from
556 household sources. *Proceedings of the National Academy of Sciences*, *116*(22), 10711–10716.
557 https://doi.org/10.1073/pnas.1900888116
558 Conibear, L., Butt, E. W., Knote, C., Arnold, S. R., & Spracklen, D. V. (2018). Residential energy use
559 emissions dominate health impacts from exposure to ambient particulate matter in India.
560 *Nature Communications*, *9*(1). https://doi.org/10.1038/s41467-018-02986-7
561 Dave, P., Bhushan, M., & Venkataraman, C. (2017). Aerosols cause intraseasonal short-term
562 suppression of Indian monsoon rainfall. *Scientific Reports*, *7*(1), 17347.
563 https://doi.org/10.1038/s41598-017-17599-1
564 David, L. M., Ravishankara, A. R., Kodros, J. K., Venkataraman, C., Sadavarte, P., Pierce, J. R., et al.
565 (2018). Aerosol Optical Depth Over India. *Journal of Geophysical Research: Atmospheres*,
566 *123*(7), 3688–3703. https://doi.org/10.1002/2017JD027719
567 Gautam, S., Yadav, A., Pillarisetti, A., Smith, K., & Arora, N. (2018). Short-Term Introduction of Air
568 Pollutants from Fireworks During Diwali in Rural Palwal, Haryana, India: A Case Study. *IOP*

569 *Conference Series: Earth and Environmental Science*, *120*, 012009.
570 https://doi.org/10.1088/1755-1315/120/1/012009
571 Guenther, A. B., Jiang, X., Heald, C. L., Sakulyanontvittaya, T., Duhl, T., Emmons, L. K., & Wang, X.
572 (2012). The Model of Emissions of Gases and Aerosols from Nature version 2.1 (MEGAN2.1): an
573 extended and updated framework for modeling biogenic emissions. *Geoscientific Model*
574 *Development*, *5*(6), 1471–1492. https://doi.org/10.5194/gmd-5-1471-2012
575 Gupta, R., Somanathan, E., & Dey, S. (2017). Global warming and local air pollution have reduced
576 wheat yields in India. *Climatic Change*, *140*(3–4), 593–604. https://doi.org/10.1007/s10584-
577 016-1878-8
578 Guttikunda, S. K., & Jawahar, P. (2014). Atmospheric emissions and pollution from the coal-fired
579 thermal power plants in India. *Atmospheric Environment*, *92*, 449–460.
580 https://doi.org/10.1016/j.atmosenv.2014.04.057
581 Huang, R. J., Zhang, Y., Bozzetti, C., Ho, K. F., Cao, J. J., Han, Y., et al. (2015). High secondary aerosol
582 contribution to particulate pollution during haze events in China. *Nature*, *514*(7521), 218–222.
583 https://doi.org/10.1038/nature13774
584 Huang, X., Ding, A., Gao, J., Zheng, B., Zhou, D., Qi, X., et al. (2020). Enhanced secondary pollution
585 offset reduction of primary emissions during COVID-19 lockdown in China. *National Science*
586 *Review*, *0*, 1–9.
587 IPCC. (2013). *CLIMATE CHANGE 2013 The Physical Science Basis*. Intergovernmental Panel on Climate
588 Change.
589 Jaeglé, L., Quinn, P. K., Bates, T. S., Alexander, B., & Lin, J.-T. (2011). Global distribution of sea salt
590 aerosols: new constraints from in situ and remote sensing observations. *Atmospheric Chemistry*
591 *and Physics*, *11*(7), 3137–3157. https://doi.org/10.5194/acp-11-3137-2011

592 Karambelas, A., Fiore, A. M., Westervelt, D.M., McNeill, V.F., Randles, C.A., Venkataraman, C., Pierce,
593 J.R., Bilsback, K.R., Milly, G.P. (2022). Investigating drivers of particulate matter pollution over
594 India and the implications for radiative forcing with GEOS-Chem-TOMAS15: Data and Code
595 [Dataset]. Columbia University Academic Commons. URL TBD.
596 Karambelas, A., Holloway, T., Kinney, P. L., Fiore, A. M., DeFries, R., Kiesewetter, G., & Heyes, C. (2018).
597 Urban versus rural health impacts attributable to PM2.5 and O3 in northern India.
598 *Environmental Research Letters*, *13*(6), 064010. https://doi.org/10.1088/1748-9326/aac24d
599 Keller, C. A., Long, M. S., Yantosca, R. M., Da Silva, A. M., Pawson, S., & Jacob, D. J. (2014). HEMCO v1.0:
600 A versatile, ESMF-compliant component for calculating emissions in atmospheric models.
601 *Geoscientific Model Development*, *7*(4), 1409–1417. https://doi.org/10.5194/gmd-7-1409-2014
602 Kodros, J. K., & Pierce, J. R. (2017). Important global and regional differences in aerosol cloud-albedo
603 effect estimates between simulations with and without prognostic aerosol microphysics:
604 DIFFERENCES IN CLOUD-ALBEDO AEROSOL INDIRECT EFFECT. *Journal of Geophysical Research:*
605 *Atmospheres*, *122*(7), 4003–4018. https://doi.org/10.1002/2016JD025886
606 Kodros, John K., Cucinotta, R., Ridley, D. A., Wiedinmyer, C., & Pierce, J. R. (2016). The aerosol radiative
607 effects of uncontrolled combustion of domestic waste. *Atmospheric Chemistry and Physics*,
608 *16*(11), 6771–6784. https://doi.org/10.5194/acp-16-6771-2016
609 Li, C., McLinden, C., Fioletov, V., Krotkov, N., Carn, S., Joiner, J., et al. (2017). India Is Overtaking China
610 as the World's Largest Emitter of Anthropogenic Sulfur Dioxide. *Scientific Reports*, *7*(1).
611 https://doi.org/10.1038/s41598-017-14639-8
612 Li, Z., Guo, J., Ding, A., Liao, H., Liu, J., Sun, Y., et al. (2017). Aerosol and boundary-layer interactions
613 and impact on air quality. *National Science Review*, *4*(6), 810–833.
614 https://doi.org/10.1093/nsr/nwx117

615 Liang et al. (2010). Finding the missing stratospheric Br_y: a global modeling study of $CHBr_3$ and CH_2Br_2,
616 Atmos. Chem. Phys., doi:10.5194/acp-10-2269-2010.
617 Liu, T., Marlier, M. E., DeFries, R. S., Westervelt, D. M., Xia, K. R., Fiore, A. M., et al. (2018). Seasonal
618 impact of regional outdoor biomass burning on air pollution in three Indian cities: Delhi,
619 Bengaluru, and Pune. *Atmospheric Environment*, *172*(September 2017), 83–92.
620 https://doi.org/10.1016/j.atmosenv.2017.10.024
621 Liu, T., Marlier, M., Karambelas, A., Jain, M., Singh, S., Singh, M., et al. (2019). Missing emissions from
622 post-monsoon agricultural fires in northwestern India: regional limitations of MODIS burned
623 area and active fire products. *Environmental Research Communications*, *1*(01), 1007.
624 https://doi.org/10.31223/osf.io/9jvak
625 Lucchesi, R. (2013). File Specification for GEOS-5 FP, *No. 4*(Version 1.0), 63.
626 Marais, E. and C. Wiedinmyer (2016). *Air quality impact of Diffuse and Inefficient Combustion Emissions*
627 *in Africa (DICE-Africa)*, Environ. Sci. Technol., 50(19), 10739–10745,
628 doi:10.1021/acs.est.6b02602.
629 McLinden, C. A., Olsen, S. C., Hannegan, B., Wild, O., Prather, M. J., & Sundet, J. (2000). Stratospheric
630 ozone in 3-D models: A simple chemistry and the cross-tropopause flux. *Journal of Geophysical*
631 *Research: Atmospheres*, *105*(D11), 14653–14665. https://doi.org/10.1029/2000JD900124
632 Mhawish, A., Banerjee, T., Sorek-Hamer, M., Lyapustin, A., Broday, D. M., & Chatfield, R. (2019).
633 Comparison and evaluation of MODIS Multi-angle Implementation of Atmospheric Correction
634 (MAIAC) aerosol product over South Asia. *Remote Sensing of Environment*, *224*, 12–28.
635 https://doi.org/10.1016/j.rse.2019.01.033

636 Mukherjee, T., Vinoj, V., Midya, S. K., Puppala, S. P., & Adhikary, B. (2020). Numerical simulations of
637 different sectoral contributions to post monsoon pollution over Delhi. *Heliyon*, *6*(3), e03548.
638 https://doi.org/10.1016/j.heliyon.2020.e03548
639 Murray, L. T., Jacob, D. J., Logan, J. A., Hudman, R. C., & Koshak, W. J. (2012). Optimized regional and
640 interannual variability of lightning in a global chemical transport model constrained by LIS/OTD
641 satellite data: IAV OF LIGHTNING CONSTRAINED BY LIS/OTD. *Journal of Geophysical Research:*
642 *Atmospheres*, *117*(D20). https://doi.org/10.1029/2012JD017934
643 Pai, S. J., Heald, C. L., Pierce, J. R., Farina, S. C., Marais, E. A., Jimenez, J. L., et al. (2020). An evaluation
644 of global organic aerosol schemes using airborne observations. *Atmos. Chem. Phys.*, 29.
645 Petters, M. D., & Kreidenweis, S. M. (2007). A single parameter representation of hygroscopic growth
646 and cloud condensation nucleus activity. *Atmos. Chem. Phys.*, 11.
647 Philip, S., Martin, R. V., Snider, G., Weagle, C. L., van Donkelaar, A., Brauer, M., et al. (2017).
648 Anthropogenic fugitive, combustion, and industrial dust is significant, underrepresented fine
649 particulate matter source in global atmospheric models. *Environmental Research Letters*,
650 *044018*. https://doi.org/10.1088/1748-9326/aa65a4
651 Pommier, M., Fagerli, H., Gauss, M., Simpson, D., Sharma, S., Sinha, V., et al. (2017). Impact of regional
652 climate change and future emission scenarios on surface O3 and PM2.5 over India. *Atmospheric*
653 *Chemistry and Physics Discussions*, *185194*, 1–41. https://doi.org/10.5194/acp-2017-519
654 Ramnarine, E., Kodros, J. K., Hodshire, A. L., Lonsdale, C. R., Alvarado, M. J., & Pierce, J. R. (2019).
655 Effects of near-source coagulation of biomass burning aerosols on global predictions of aerosol
656 size distributions and implications for aerosol radiative effects. *Atmospheric Chemistry and*
657 *Physics*, *19*(9), 6561–6577. https://doi.org/10.5194/acp-19-6561-2019

Ravishankara, A. R., David, L. M., Pierce, J. R., & Venkataraman, C. (2020). Outdoor air pollution in India is not only an urban problem. *Proceedings of the National Academy of Sciences*, *117*(46), 28640–28644. https://doi.org/10.1073/pnas.2007236117

Rosenfeld, D., et al. (2008), Flood or drought: How do aerosols affect precipitation?. *Science*, **321**, 1309–1313. https://doi:10.1126/science.1160606.

Roozitalab, B., Carmichael, G. R., & Guttikunda, S. K. (2020). *Improving regional air quality predictions in the Indo-Gangetic Plain-Case study of an intensive pollution episode in November 2017* (preprint). Aerosols/Atmospheric Modelling/Troposphere/Chemistry (chemical composition and reactions). https://doi.org/10.5194/acp-2020-744

Schnell, J. L., Naik, V., Horowitz, L. W., Paulot, F., Mao, J., Ginoux, P., et al. (2018). Exploring the relationship between surface PM2.5 and meteorology in Northern India. *Atmospheric Chemistry and Physics*, *18*(14), 10157–10175. https://doi.org/10.5194/acp-18-10157-2018

Sherwen, T., Schmidt, J. A., Evans, M. J., Carpenter, L. J., Großmann, K., Eastham, S. D., et al. (2016). Global impacts of tropospheric halogens (Cl, Br, I) on oxidants and composition in GEOS-Chem. *Atmospheric Chemistry and Physics*, *16*(18), 12239–12271. https://doi.org/10.5194/acp-16-12239-2016

Shi, X., & Brasseur, G. P. (2020). The Response in Air Quality to the Reduction of Chinese Economic Activities During the COVID-19 Outbreak. *Geophysical Research Letters*, *47*(11). https://doi.org/10.1029/2020GL088070

Slater, J., Coe, H., McFiggans, G., Tonttila, J., & Romakkaniemi, S. (2022). The effect of BC on aerosol–boundary layer feedback: potential implications for urban pollution episodes. *Atmospheric Chemistry and Physics*, *22*(4), 2937–2953. https://doi.org/10.5194/acp-22-2937-2022

680 Stettler, M. E. J., Eastham, S., & Barrett, S. R. H. (2011). Air quality and public health impacts of UK
681 airports. Part I: Emissions. *Atmospheric Environment*, *45*(31), 5415–5424.
682 https://doi.org/10.1016/j.atmosenv.2011.07.012
683 Stohl, A., Aamaas, B., Amann, M., Baker, L. H., Bellouin, N., Berntsen, T. K., et al. (2015). Evaluating the
684 climate and air quality impacts of short-lived pollutants. *Atmospheric Chemistry and Physics*,
685 *15*(18), 10529–10566. https://doi.org/10.5194/acp-15-10529-2015
686 Tzompa-Sosa, Z. A., Mahieu, E., Franco, B., Keller, C. A., Turner, A. J., Helmig, D., et al. (2017). Revisiting
687 global fossil fuel and biofuel emissions of ethane. *Journal of Geophysical Research:*
688 *Atmospheres*, *122*(4), 2493–2512. https://doi.org/10.1002/2016JD025767
689 Twomey, S., The influence of pollution on the short wave albedo of clouds, *J. Atmos. Sci.*, **34**, 1149–
690 1152, 1977.
691 Van Der Werf, G. R., Randerson, J. T., Giglio, L., Collatz, G. J., Mu, M., Kasibhatla, P. S., et al. (2010).
692 Global fire emissions and the contribution of deforestation, savanna, forest, agricultural, and
693 peat fires (1997-2009). *Atmospheric Chemistry and Physics*, *10*(23), 11707–11735.
694 https://doi.org/10.5194/acp-10-11707-2010
695 Venkataraman, C., Brauer, M., Tibrewal, K., Sadavarte, P., Ma, Q., Cohen, A., et al. (2018). Source
696 influence on emission pathways and ambient PM2.5 pollution over India (2015-2050).
697 *Atmospheric Chemistry and Physics Discussions*, (December), 1–38.
698 https://doi.org/10.5194/acp-2017-1114
699 Vinken, G. C. M., Boersma, K. F., Jacob, D. J., & Meijer, E. W. (2011). Accounting for non-linear
700 chemistry of ship plumes in the GEOS-Chem global chemistry transport model. *Atmospheric*
701 *Chemistry and Physics*, *11*(22), 11707–11722. https://doi.org/10.5194/acp-11-11707-2011

Wang, L. T., Wei, Z., Yang, J., Zhang, Y., Zhang, F. F., Su, J., et al. (2014). The 2013 severe haze over southern Hebei, China: Model evaluation, source apportionment, and policy implications. *Atmospheric Chemistry and Physics*, *14*(6), 3151–3173. https://doi.org/10.5194/acp-14-3151-2014

Wang, Y., Xia, W., Liu, X. *et al.* Disproportionate control on aerosol burden by light rain. *Nat. Geosci.* **14,** 72–76 (2021). https://doi.org/10.1038/s41561-020-00675-z

Westervelt, D. M., You, Y., Li, X., Ting, M., Lee, D. E., & Ming, Y. (2020). Relative Importance of Greenhouse Gases, Sulfate, Organic Carbon, and Black Carbon Aerosol for South Asian Monsoon Rainfall Changes. *Geophysical Research Letters*, *47*(13). https://doi.org/10.1029/2020GL088363

Wiedinmyer, C., Yokelson, R. J., & Gullett, B. K. (2014). Global Emissions of Trace Gases, Particulate Matter, and Hazardous Air Pollutants from Open Burning of Domestic Waste. *Environmental Science & Technology*, *48*(16), 9523–9530. https://doi.org/10.1021/es502250z

Wilcox, E. M., Thomas, R. M., Praveen, P. S., Pistone, K., Bender, F. A.-M., & Ramanathan, V. (2016). Black carbon solar absorption suppresses turbulence in the atmospheric boundary layer. *Proceedings of the National Academy of Sciences*, *113*(42), 11794–11799. https://doi.org/10.1073/pnas.1525746113

Xia, W., Wang, Y., Chen, S., Huang, J., Wang, B., Zhang, G. J., et al. (2022). Double Trouble of Air Pollution by Anthropogenic Dust. *Environmental Science & Technology*, *56*(2), 761–769. https://doi.org/10.1021/acs.est.1c04779

Figures and Tables

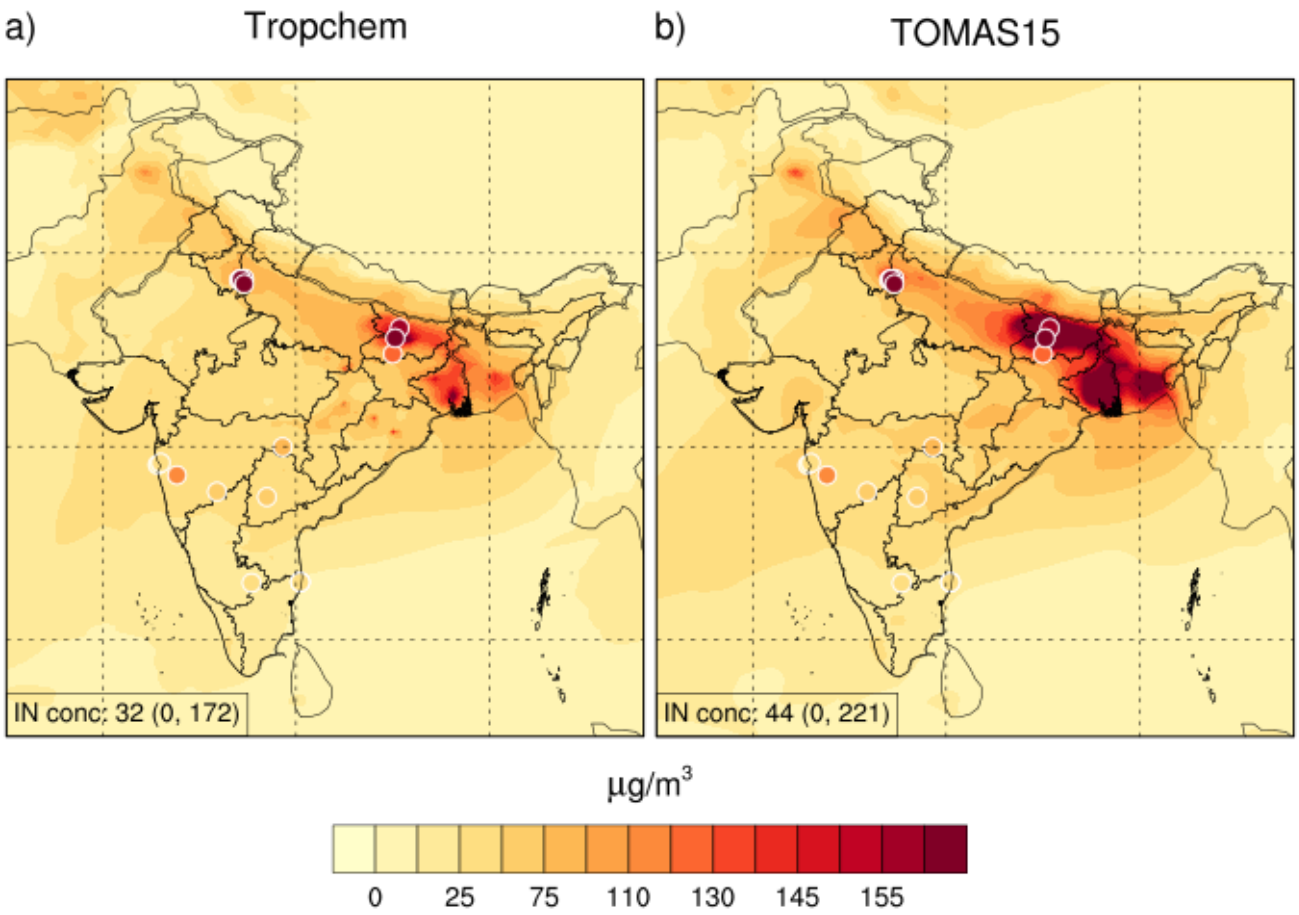

Figure 1 Average $PM_{2.5}$ concentrations during the December 5-9 2015 episode simulated with the regionally nested high-resolution GEOS-Chem model over India for a) Tropchem and b) GC-TOMAS15 overlaid with observations from the CPCB. The values in the lower left indicate the model area average (in µg/m^3) and full range within India

	Model Average (µg/m^3)	**Observed Average µg/m^3)**	**# Points**	**Mean Fractional Bias**	**Normalized Mean Bias**	**Normalized Mean Error**	**r^2**
Tropchem 2x2.5 (December episode)	47 (64)	144 (142)	22 (18)	-95% (-63%)	-67% (-55%)	67% (56%)	0.60 (0.40)
GC-TOMAS15 2x2.5 (December episode)	58 (80)	144 (142)	22 (18)	-79% (-45%)	-59% (-44%)	60% (47%)	0.59 (0.36)
Tropchem 0.25x0.3125 (December episode)	69 (95)	144 (142)	22 (18)	-71% (-40%)	-52% (-33%)	52% (36%)	0.49 (0.69)
GC-TOMAS15 0.25x0.3125 (December episode *only*)	(125)	(142)	(18)	(-16%)	(-12%)	(34%)	(0.67)

Table 1 Model evaluation of $PM_{2.5}$ with all available CPCB observations in India averaged over the October-November-December season or during the December 5-9 2015 pollution episode as shown in parentheses. Correlations are spatial.

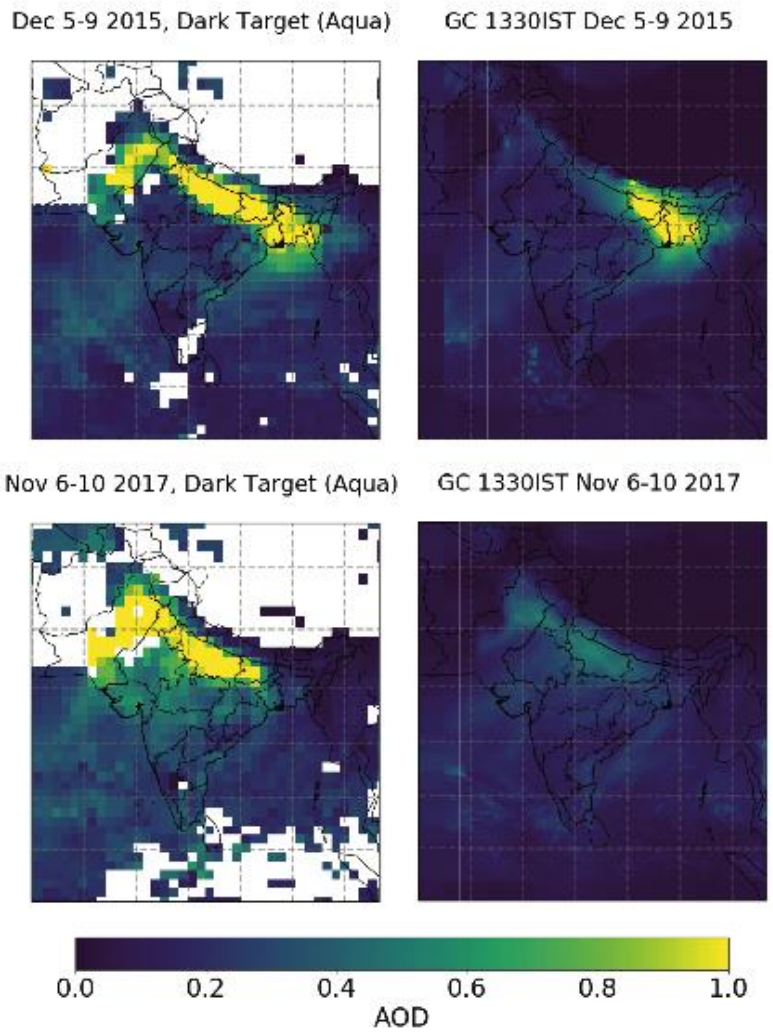

Figure 2. AOD from MODIS Aqua (left column; Dark Target retrieval algorithm) compared with GC-TOMAS15 1:30 PM local time averaged for each pollution episode (right column) during December 5-9 2015 (top row) and November 6-10 2017 (bottom row).

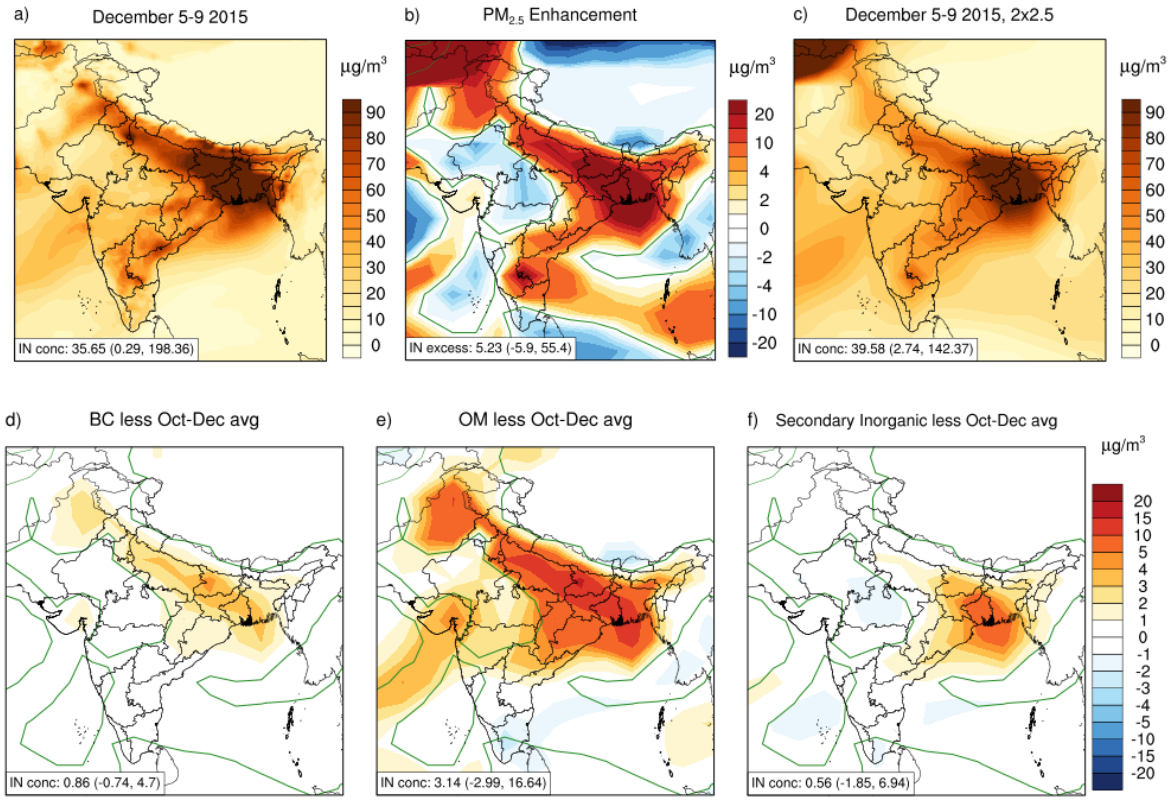

Figure 3 a) Average December 5-9 2015 episode $PM_{2.5}$ concentration (0.25 x 0.3125 GC-TOMAS15); and concentration enhancements during the episode relative to seasonal average for (all 2 x 2.5) b) $PM_{2.5}$ c) average December 5-9 2015 episode $PM_{2.5}$ concentrations in the 2 x 2x.5 simulation d) black carbon (BC) e) organic matter (OM); f) the sum of inorganic aerosols (sulfate, nitrate, and ammonium). A single contour denoting zero change in total $PM_{2.5}$ is superimposed in green.

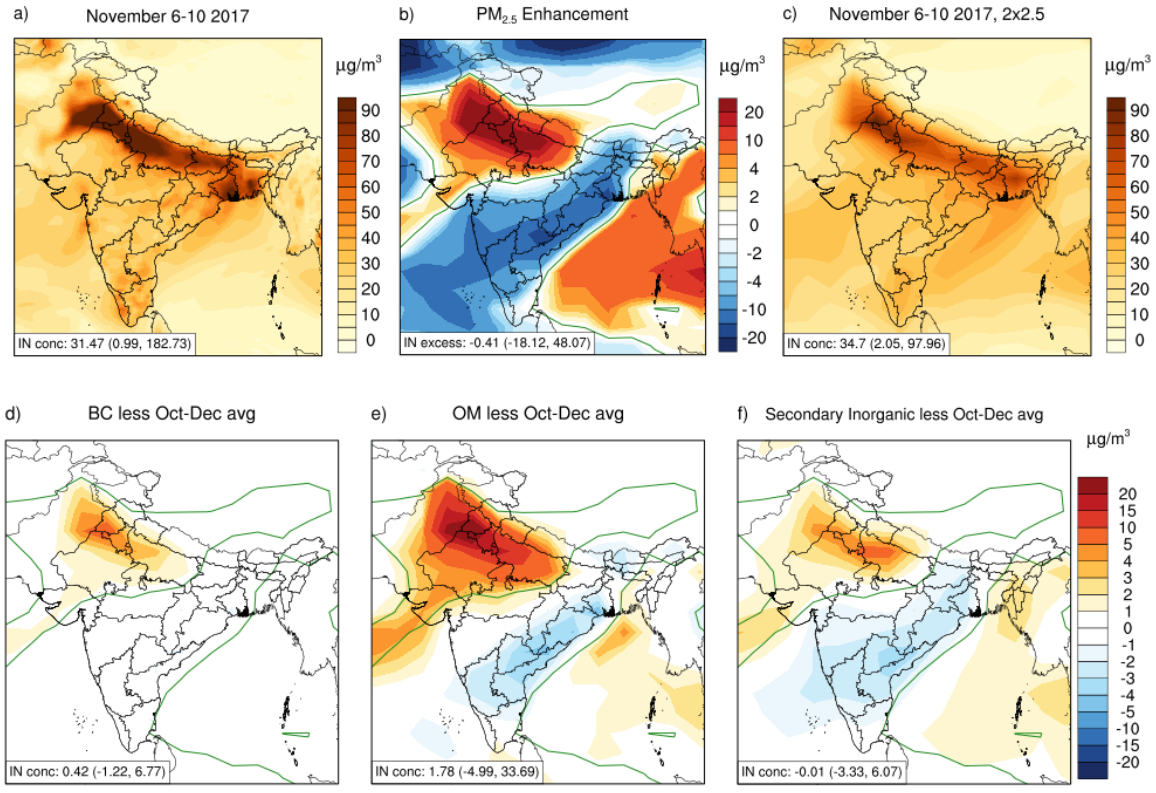

Figure 4 Same as Figure 3 except for the November 6-10 2017 episode.

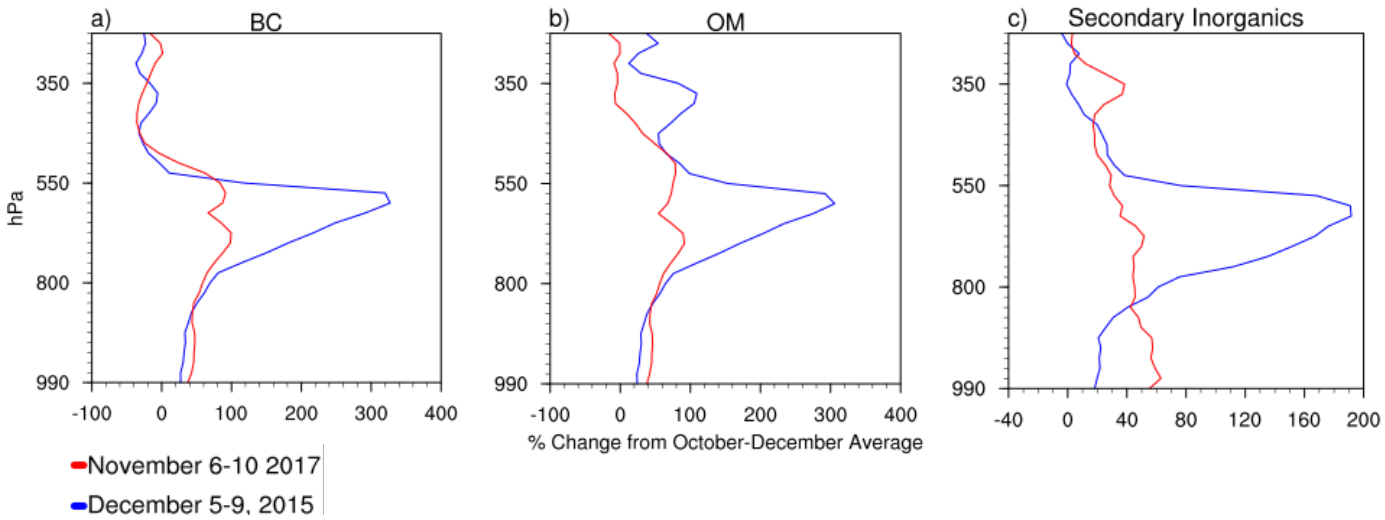

Figure 5 Average concentration differences in the column above regions where the surface $PM_{2.5}$ episodic enhancement is positive, for (a) black carbon, (b) organic matter, and (c) secondary inorganic aerosol. The red lines are for the relative (%) change of the 2017 episode from the 2017 October to December average and blue shows the relative (%) change of the 2015 episode from the 2015 October to December average.

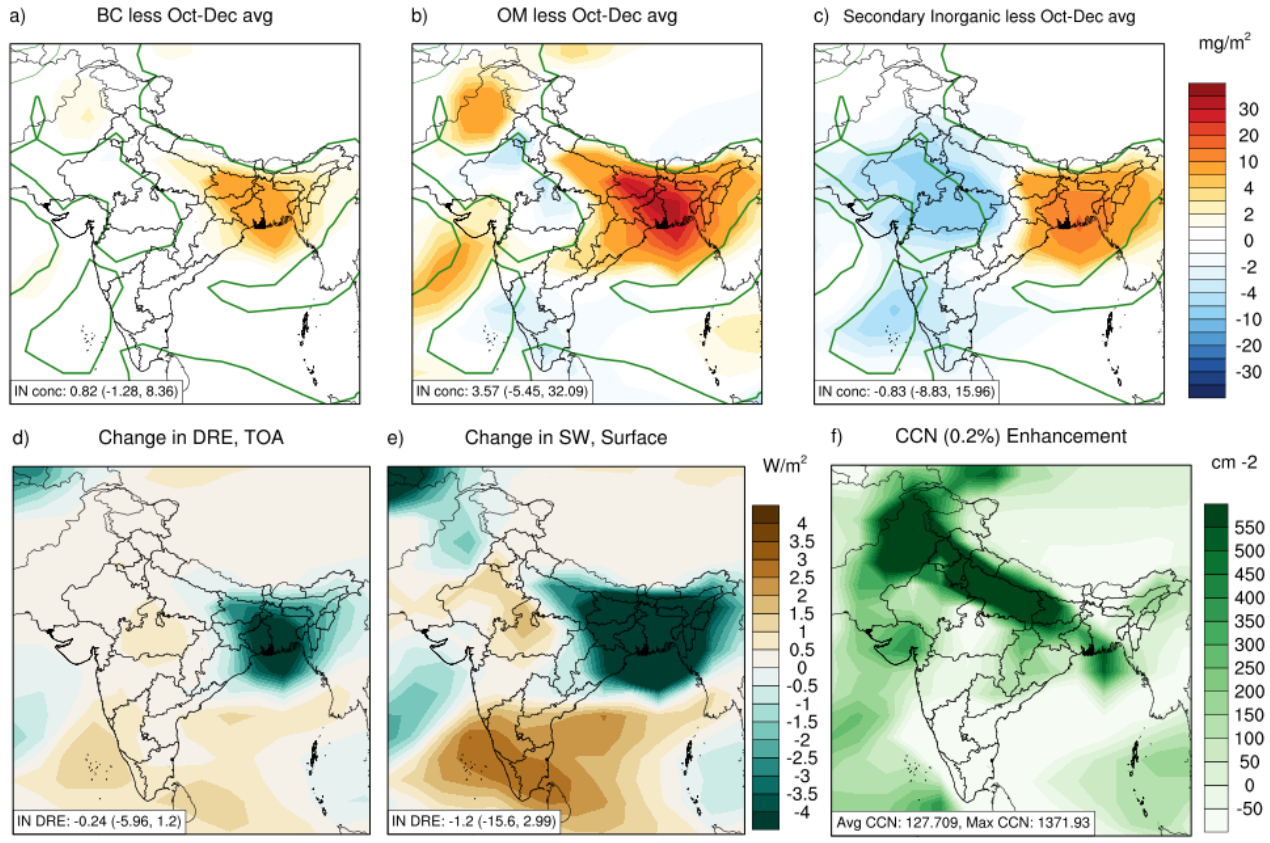

Figure 6 Changes in the column burdens of a) black carbon b) organic matter c) secondary inorganics during the December 5-9, 2015 pollution episode from seasonal average (October-December) in the GC-TOMAS15 coarse horizontal resolution (global) simulations (seasonal fields are only available at coarse resolution). Also shown are changes during the episode from the seasonal mean of d) direct radiative effect (DRE) at the top of the atmosphere (TOA); e) net surface shortwave (SW) radiation; f) total column cloud condensation nuclei (0.2% supersaturation). The singular contour for zero change is shown in green. Negative DRE and SW are indicative of cooling.

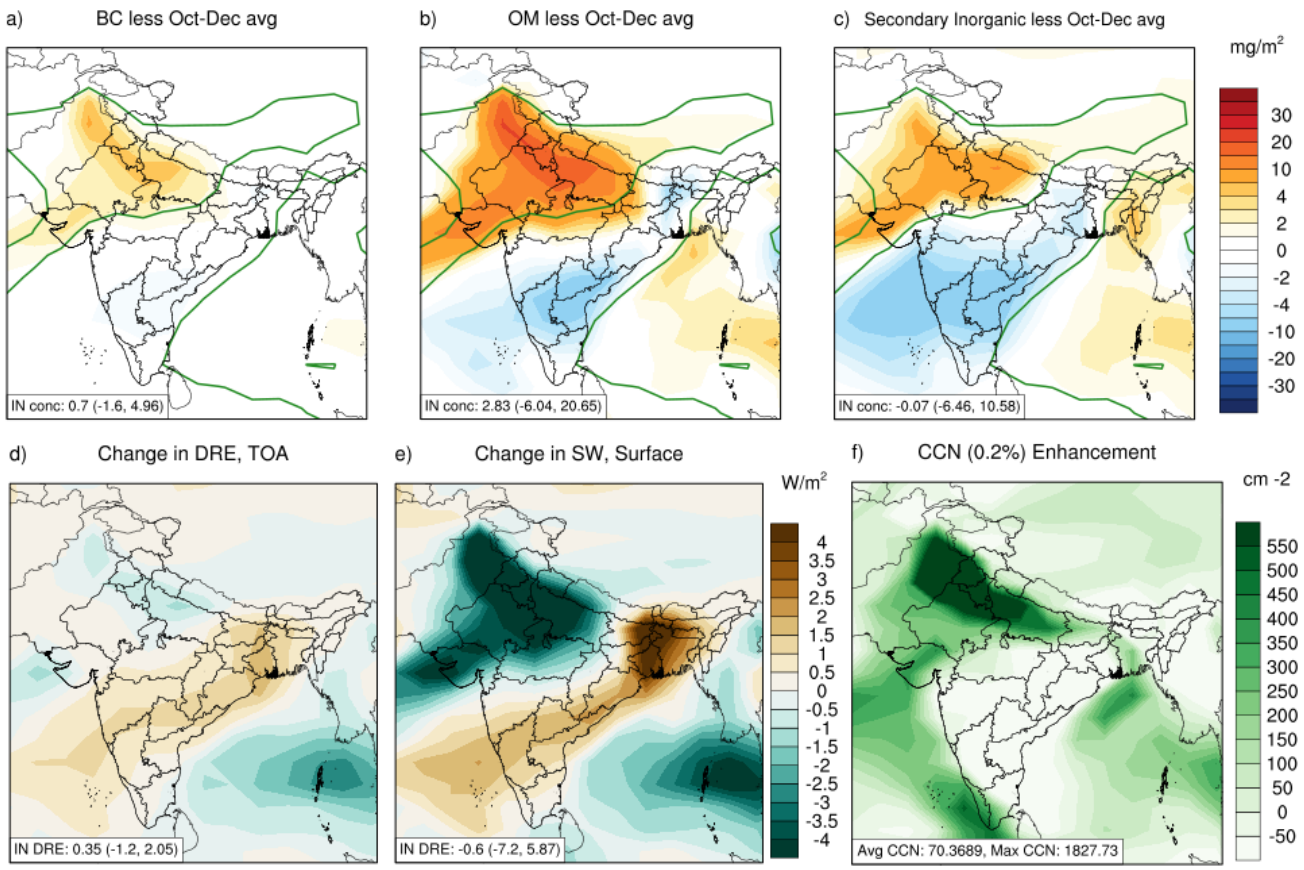

Figure 7 Same as Figure 6 except for the November 6-10, 2017 episode.

Journal of Geophysical Research – Atmospheres

Supporting Information for

Investigating drivers of particulate matter pollution over India and the implications for radiative forcing with GEOS-Chem-TOMAS15

Authors: Alexandra Karambelas[1,*], Arlene M. Fiore[1,2,^], Daniel M. Westervelt[1,7], V. Faye McNeill[3], Cynthia A. Randles[4], Chandra Venkataraman[5], Jeffrey R. Pierce[6], Kelsey R. Bilsback[6], George P. Milly[1]

[1] Lamont-Doherty Earth Observatory, Columbia University, Palisades, NY USA
* Now at Northeast States for Coordinated Air Use Management, Boston, MA USA
[2] Department of Earth and Environmental Sciences, Columbia University, New York, NY USA
^Now at Department of Earth, Atmospheric and Planetary Sciences, Massachusetts Institute of Technology, Cambridge, MA, USA
[3] Chemical and Environmental Engineering, Columbia University, New York, NY USA
[4] ExxonMobil Technology and Engineering Company, Annandale, NJ USA
[5] Department of Chemical Engineering, Indian Institute of Technology Bombay, Mumbai, India
[6] Department of Atmospheric Science, Colorado State University, Fort Collins, CO USA
[7] NASA Goddard Institute for Space Studies, New York, NY, USA

Contents of this file

Detailed information on GEOS-Chem

We use GEOS-Chem v12.0.2 for all global and nested India simulations. Emissions mostly follow standard GEOS-Chem simulations that use HEMCO (Keller et al., 2014). A summary is included below, but more details on the emissions and HEMCO including additional references are available at http://wiki.seas.harvard.edu/geos-chem/index.php/The_HEMCO_User%27s_Guide#References.

Anthropogenic emissions for GC-Tropchem and GC-TOMAS15 simulation include ECLIPSE v5a global emissions inventory. We apply the following emissions overlays in the global simulation: hourly NEI 2011 emissions for the U.S., BRAVO emissions for Mexico, APEI emissions for Canada, EMEP emissions for Europe, and DICE emissions for Africa (Marais and Wiedinmyer, 2016). Supplemental inventories include AEIC aircraft emissions (Stettler et al., 2011), POET ethanol (EOH) emissions, Liang bromocarbon emission (Liang et al., 2012), iodocarbon emissions from Ordonez (Sherwen et al., 2016 and references therein), emissions from decaying plants, global ship emissions from ARCTAS, ICOADS, and EMAP, and volcanic eruption and degassing emissions as relevant, and ethane (C2H6) overwritten according to Tzompa-Sosa et al., (2017) for biofuel and anthropogenic sources. We also include the following extensions: SeaFlux, ship emissions (ParaNOx; Vinken et al., 2011), lightning NO_X from global lightning flash distributions (LightNOx; Murray et al., 2012), Dust Entrainment and Deposition (DEAD) scheme allocated to TOMAS15 size bins (Jaeglé et al., 2011), SeaSalt, online MEGAN emissions (Guenther et al., 2012). Biomass burning emissions were from the Global Fire Emissions Database v4 (GFED4) (Van Der Werf et al., 2010) with updated seasonal fire counts following Liu et al., (2019). Trash burning (Wiedinmyer et al. 2014) and anthropogenic fugitive dust (Philip et al., 2017) were only included in the Tropchem runs.

For nested India simulations, the regional emissions inventories for the U.S., Mexico, Canada, Europe, and Africa are not necessary as these regions fall outside the nested domain.

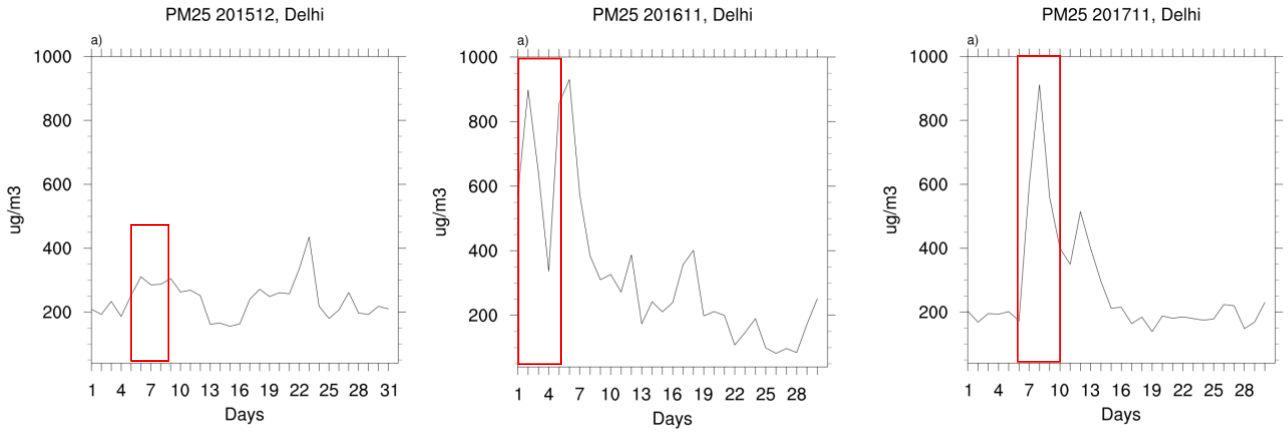

Supplemental Figure 1 Concentrations from the U.S. Embassy in Delhi during December 2015 and November 2016 and 2017. Days in red boxes were chosen to correspond with increases in concentration relative to nearby days.

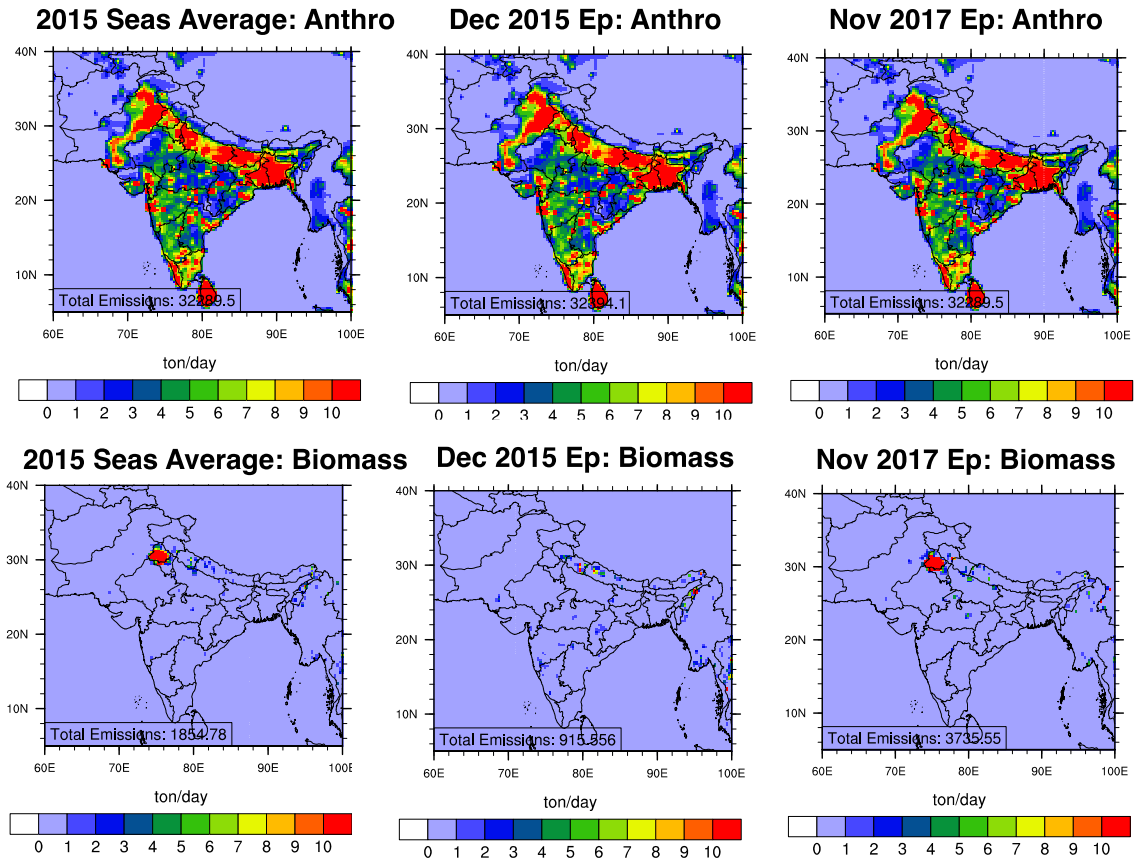

Supplemental Figure 2 Daily average OC emissions for anthropogenic sources (top row) and biomass burning (bottom row) for October to December 2015 (first column), the December 2015 episode (middle column), and the November 2017 episode (right column).

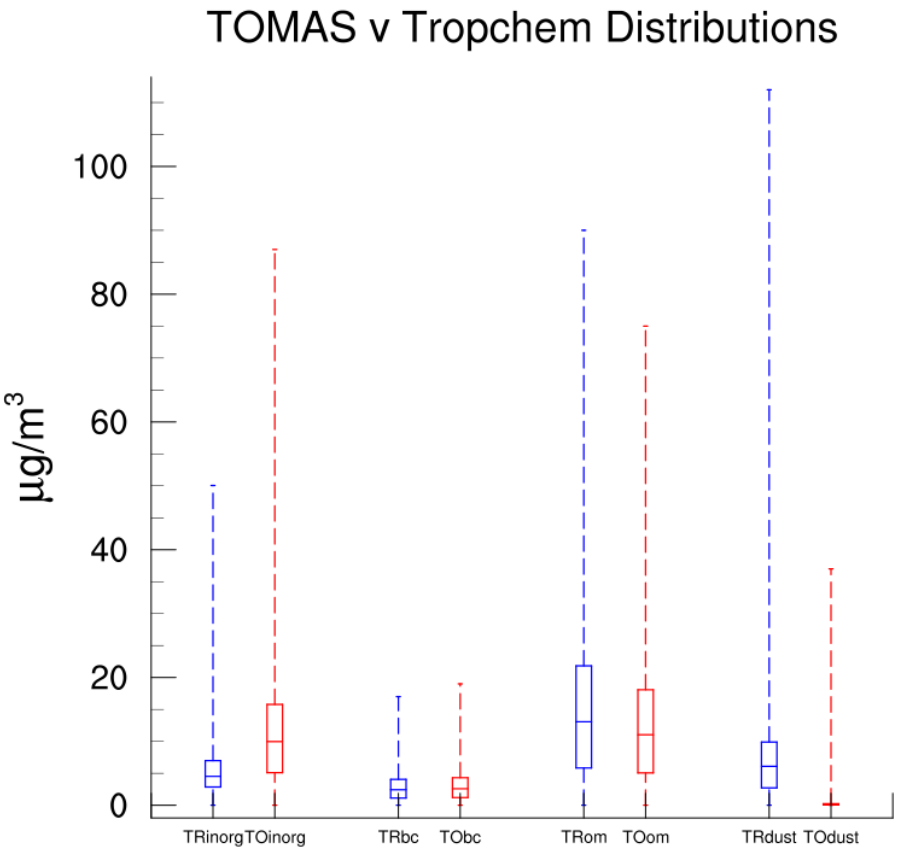

Supplemental Figure 3 Episodic average concentration distribution (minimum, 25th percentile, median, 75th percentile, maximum) for India from the GC-Tropchem (TR) and GC-TOMAS15 (TO) simulations for inorganics (inorg), black carbon (BC), organic matter (OM), and dust. The y-axis is units in µg/m^3. Largest differences occur in dust because the fugitive dust size distribution has not yet been evaluated in TOMAS.

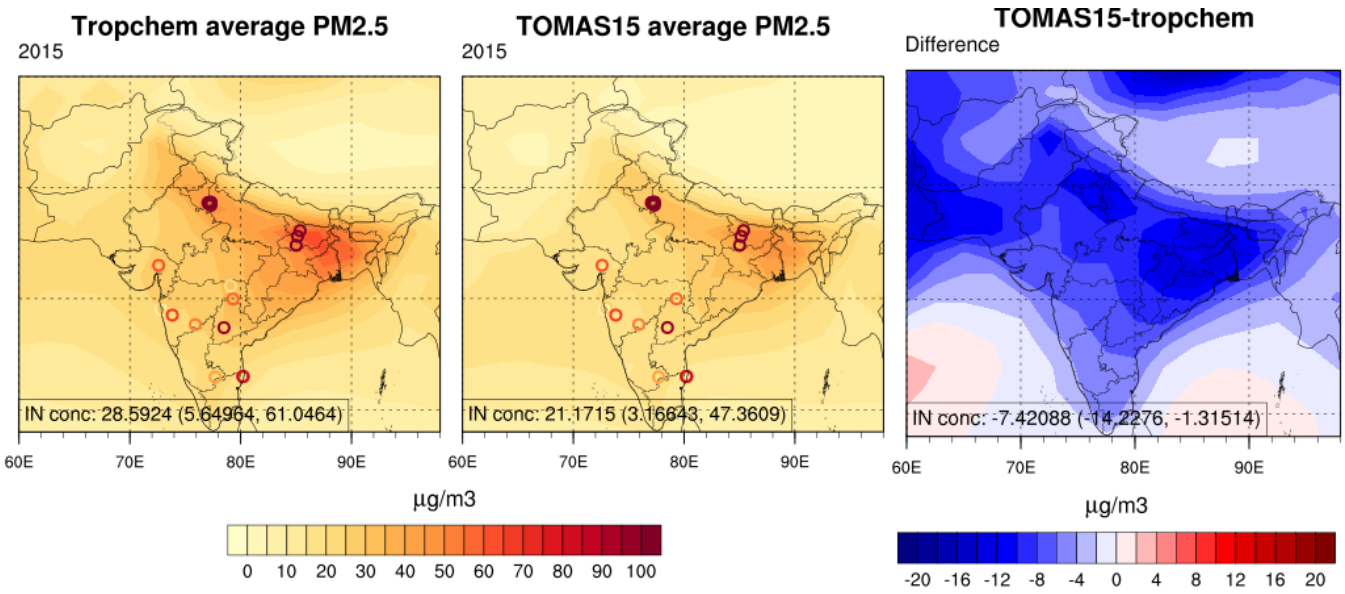

Supplemental Figure 4 Both Tropchem and TOMAS15 global simulations at 2x2.5 horizontal resolution underestimate observed $PM_{2.5}$ concentrations by at least 70 ug/m^3 in the coarse resolution model, yet spatial correlations remain high across the 24 monitor locations ($r^2_{Tropchem}$=0.81 and $r^2_{TOMAS15}$=0.80). The TOMAS15 coarse resolution simulation is systematically lower than Tropchem.

Temporal (e.g. daily average) model evaluation for October-December (Annual) 2015

	Model Average ($\mu g/m^3$)	**Observed Average $\mu g/m^3$)**	**# Points**	**Mean Fractional Bias**	**Normalized Mean Bias**	**Normalized Mean Error**	**r^2**
GC tropchem 2x2.5 (Annual)	48 (36)	139 (98)	1626 (4774)	-76% (-63%)	-66% (-63%)	66% (66%)	0.14 (0.07)
GC TOMAS 2x2.5 (Annual)	59 (38)	139 (98)	1626 (4774)	-60% (-66%)	-58% (-61%)	60% (65%)	0.13 (0.06)
GC tropchem 0.25x0.3125 (Annual)	70 (50)	139 (98)	1626 (4774)	-55% (-45%)	-50% (-49%)	55% (58%)	0.11 (0.06)

Supplemental Table 1 Model evaluation for the October-December daily average across the October to December season with annual comparisons in parenthesis. Correlations are temporal. "Model average" refers to the comparable model average concentration at observation locations.

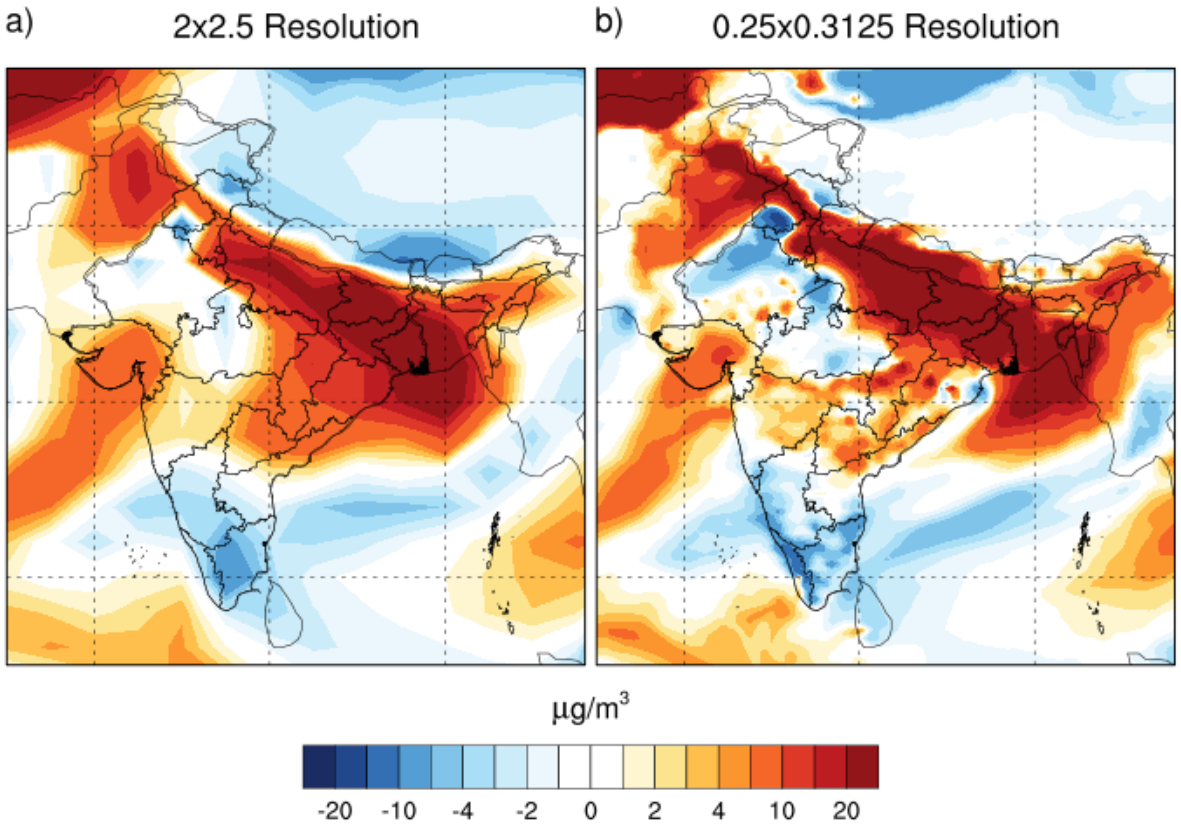

Supplemental Figure 5 Difference plots of the coarse and high resolution simulations using Tropchem for the 2015 pollution episode. Maximum (average) seasonal average concentrations for India are 85.4 $\mu g/m^3$ (32.3 $\mu g/m^3$) for the coarse resolution and 149.4 $\mu g/m^3$ (27.4 $\mu g/m^3$) for the high resolution, and maximum (average) episodic average concentrations are 133.2 $\mu g/m^3$ (38.9 $\mu g/m^3$) for the coarse resolution and 171.7 $\mu g/m^3$ (32.5 $\mu g/m^3$) for the high resolution simulation.

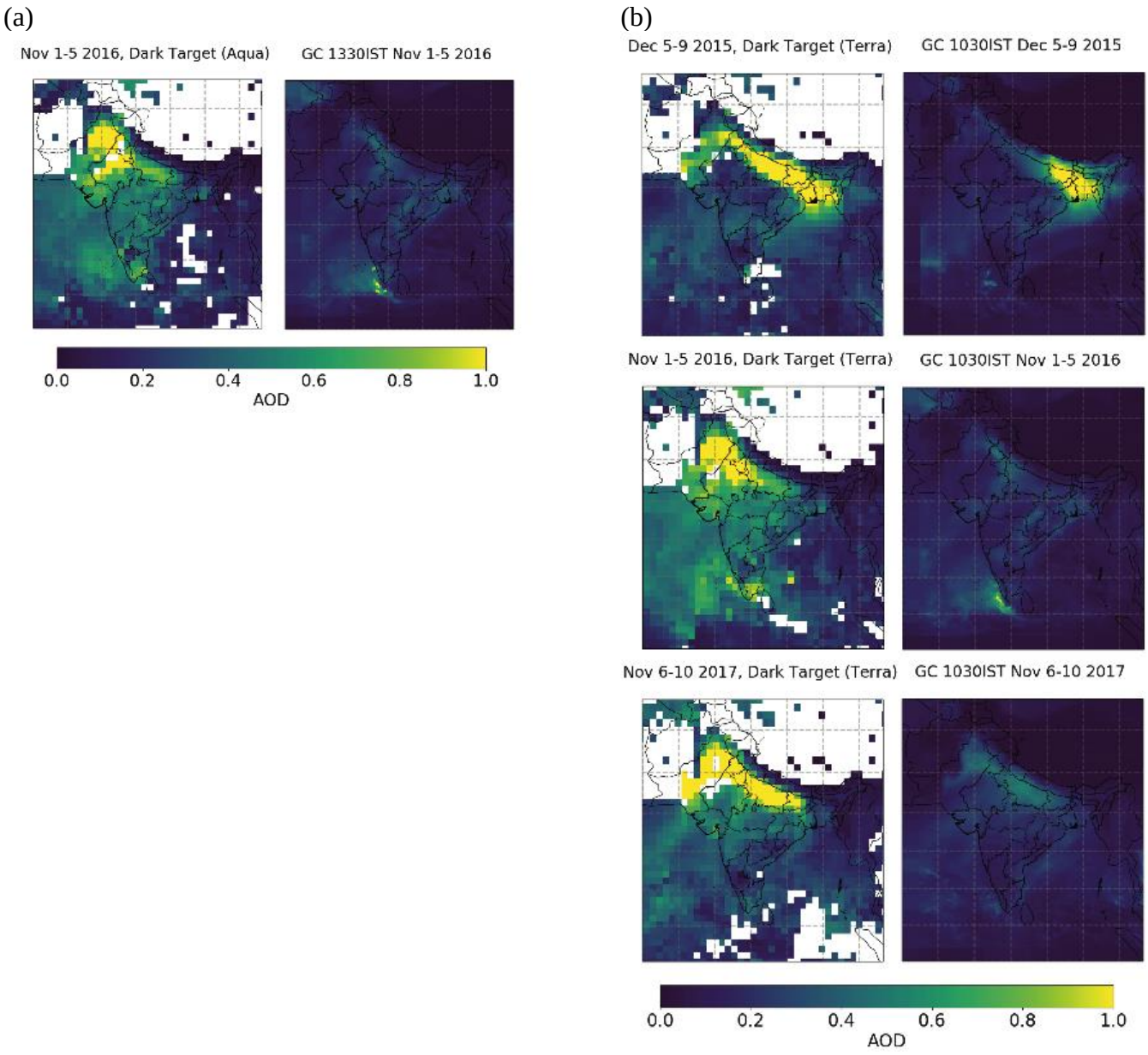

Supplemental Figure 6: MODIS AOD comparison for the (a) November 1-5 2016 pollution episode with MODIS Aqua (see Figure 2 in main text for the other two pollution episodes and (b) for all pollution episodes with MODIS Terra.

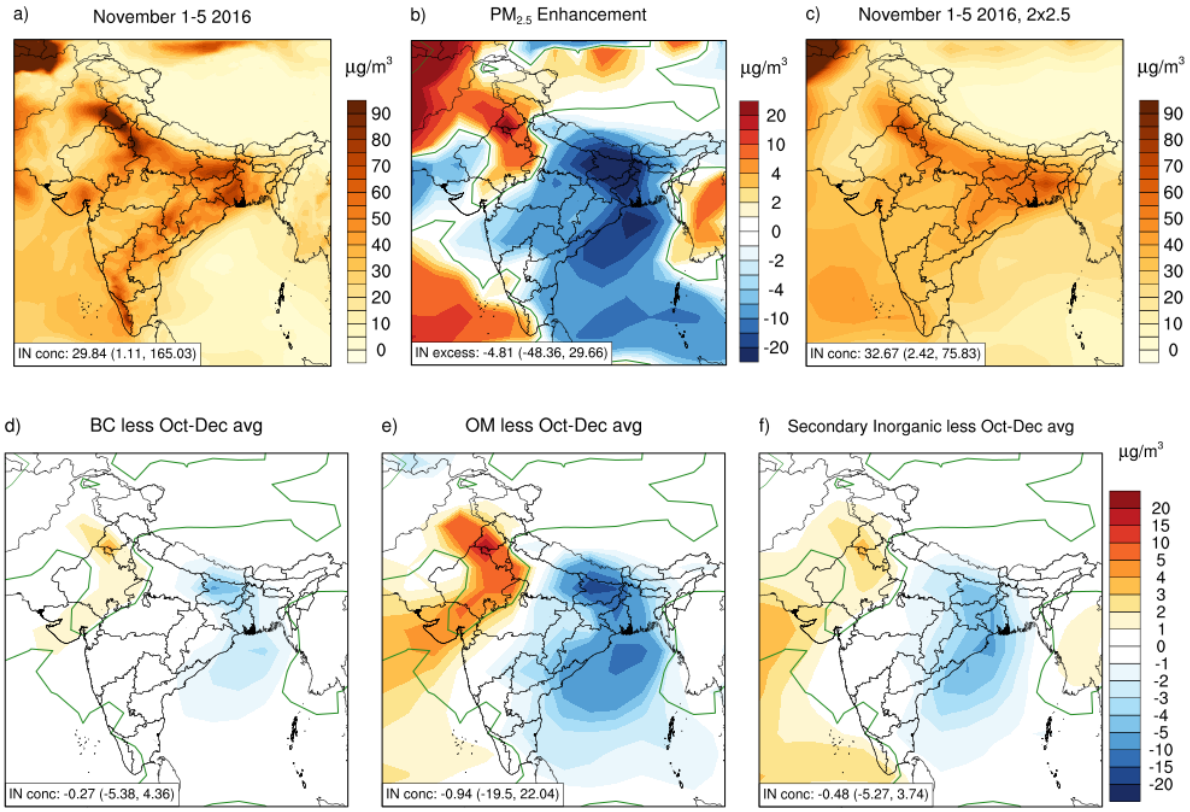

Supplemental Figure 7: Average November 1-5, 2016 episode $PM_{2.5}$ concentration (0.25 x 0.3125 GC-TOMAS15); and concentration enhancements during the episode relative to seasonal average for (all 2 x 2.5) b) $PM_{2.5}$ c) average November 1-5 2016 episode $PM_{2.5}$ concentrations in the 2 x 2x.5 simulation d) black carbon (BC) e) organic matter (OM); f) the sum of inorganic aerosols (sulfate, nitrate, and ammonium). A single contour denoting zero change is superimposed in green.

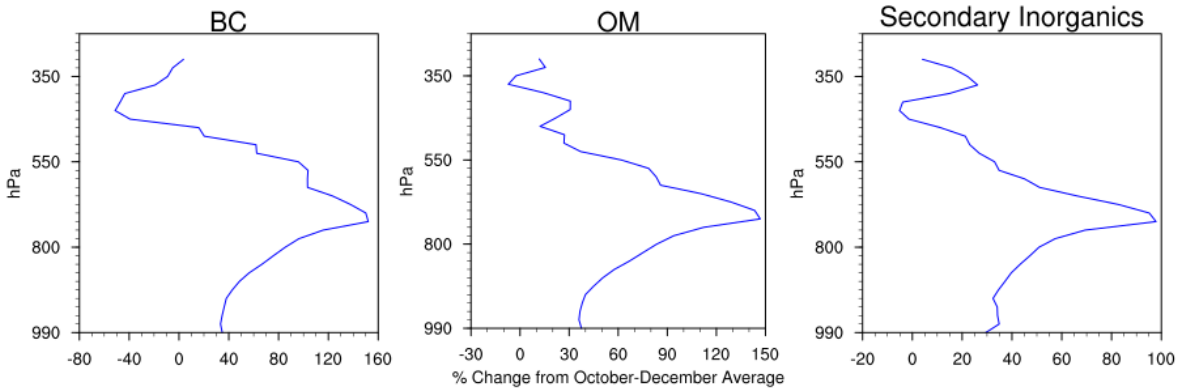

Supplemental Figure 8 Same as Figure 5 except for the November 1-5 2016 episode. Vertical gray bars at 0% indicate no change from seasonal average. Note x-axes ranges indicate smaller changes than for the 2015 and 2017 episodes.

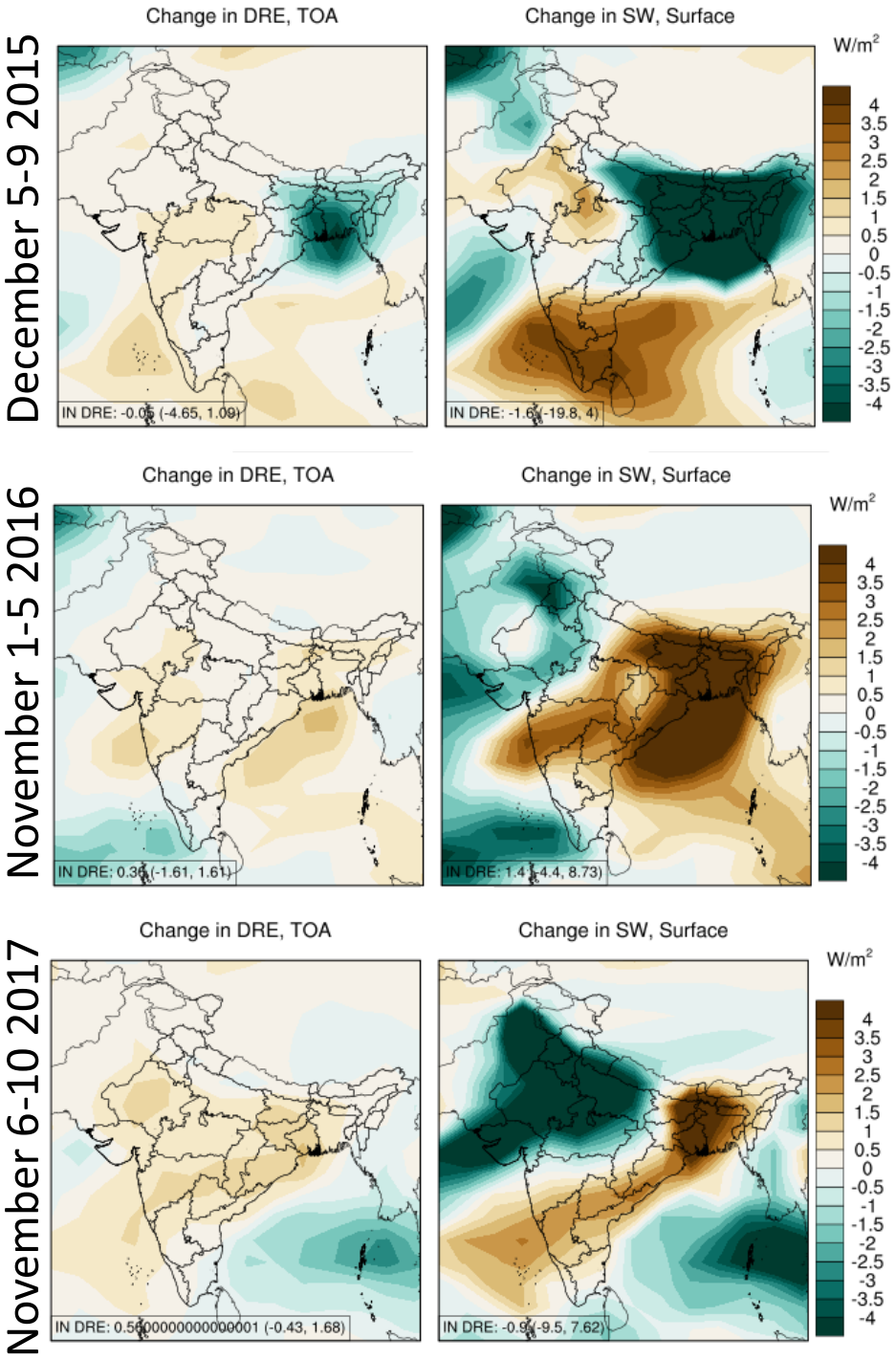

Supplemental Figure 9 RRTMG DRE core-shell between episodes and annual average for (a) 2015 and (b) 2016, and (c) 2017. Negative DRE and SW are indicative of local cooling.

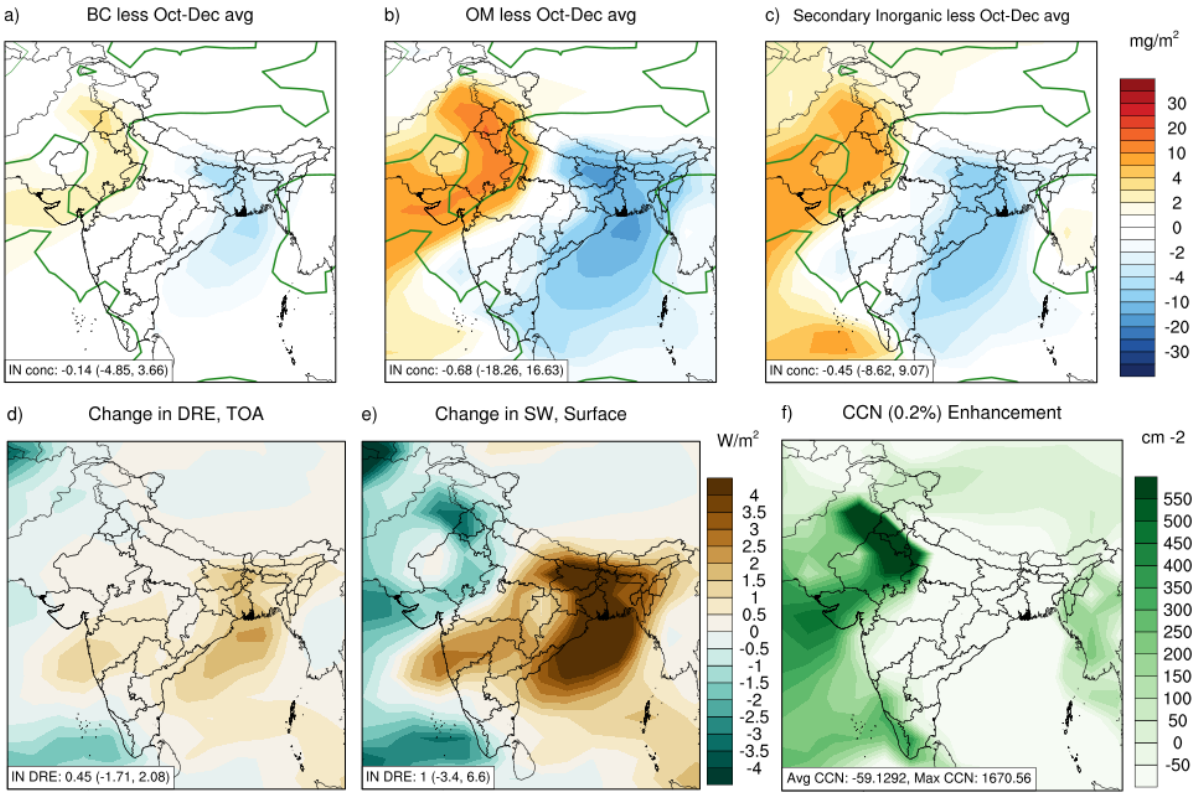

Supplemental Figure 10 Changes in the column burdens of a) black carbon b) organic matter c) secondary inorganics during the November 1-5, 2016 pollution episode from seasonal average (October-December) in the GC-TOMAS15 coarse horizontal resolution (global) simulations (seasonal fields are only available at coarse resolution). Also shown are changes during the episode from the seasonal mean of d) direct radiative effect (DRE) at the top of the atmosphere (TOA); e) net surface shortwave (SW) radiation; f) total column cloud condensation nuclei (0.2% supersaturation). Singular green contour show the line of zero change. Negative DRE and SW are indicative of cooling.

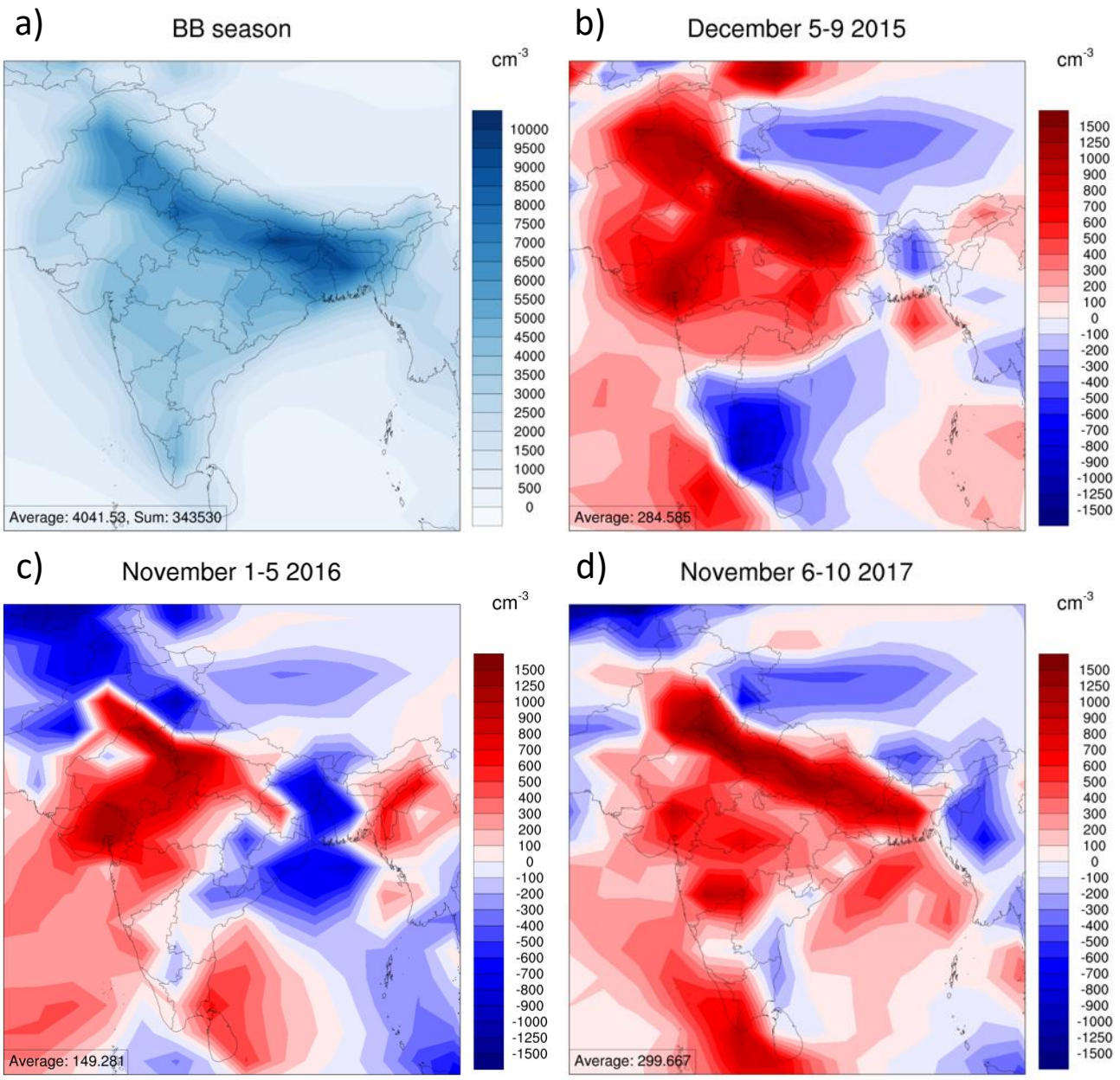

Supplemental Figure 11 Aerosol number concentration for the 2015 biomass burning season (October, November, and December) average, and the change in 2015 episode, 2016 episode, and 2017 episode from respective seasonal average. Distributions during pollution episodes are similar. The total aerosol number concentrations in India increases by approximately 8% (bottom left of each plot), from the biomass burning seasonal average.

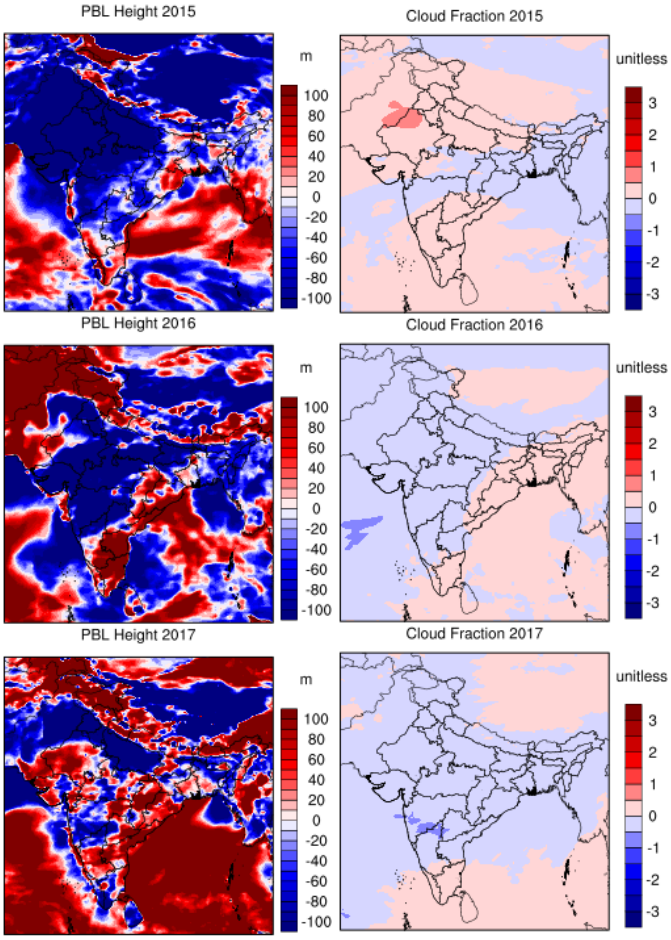

Supplemental Figure 12 Changes in meteorological variables during each episode. Differences between episode and biomass burning seasonal averages (October, November and December) for planetary boundary layer (PBL) height (left column) and cloud fraction (right column).

References

Guenther, A. B., Jiang, X., Heald, C. L., Sakulyanontvittaya, T., Duhl, T., Emmons, L. K., & Wang, X. (2012). The Model of Emissions of Gases and Aerosols from Nature version 2.1 (MEGAN2.1): an extended and updated framework for modeling biogenic emissions. *Geoscientific Model Development*, *5*(6), 1471–1492. https://doi.org/10.5194/gmd-5-1471-2012

Jaeglé, L., Quinn, P. K., Bates, T. S., Alexander, B., & Lin, J.-T. (2011). Global distribution of sea salt aerosols: new constraints from in situ and remote sensing observations. *Atmospheric Chemistry and Physics*, *11*(7), 3137–3157. https://doi.org/10.5194/acp-11-3137-2011

Keller, C. A., Long, M. S., Yantosca, R. M., Da Silva, A. M., Pawson, S., & Jacob, D. J. (2014). HEMCO v1.0: A versatile, ESMF-compliant component for calculating emissions in atmospheric models. *Geoscientific Model Development*, *7*(4), 1409–1417. https://doi.org/10.5194/gmd-7-1409-2014

Liang et al. (2010). Finding the missing stratospheric Br_y: a global modeling study of $CHBr_3$ and CH_2Br_2, Atmos. Chem. Phys., doi:10.5194/acp-10-2269-2010.

Liu, T., Marlier, M., Karambelas, A., Jain, M., Singh, S., Singh, M., et al. (2019). Missing emissions from post-monsoon agricultural fires in northwestern India: regional limitations of MODIS burned area and active fire products. *Environmental Research Communications*, *1*(01), 1007. https://doi.org/10.31223/osf.io/9jvak

Marais, E. and C. Wiedinmyer (2016). *Air quality impact of Diffuse and Inefficient Combustion Emissions in Africa (DICE-Africa)*, Environ. Sci. Technol., 50(19), 10739–10745, doi:10.1021/acs.est.6b02602.

Murray, L. T., Jacob, D. J., Logan, J. A., Hudman, R. C., & Koshak, W. J. (2012). Optimized regional and interannual variability of lightning in a global chemical transport model constrained by LIS/OTD satellite data: IAV OF LIGHTNING CONSTRAINED BY LIS/OTD. *Journal of Geophysical Research: Atmospheres*, *117*(D20). https://doi.org/10.1029/2012JD017934

Philip, S., Martin, R. V., Snider, G., Weagle, C. L., van Donkelaar, A., Brauer, M., et al. (2017). Anthropogenic fugitive, combustion, and industrial dust is significant, underrepresented fine particulate matter source in global atmospheric models. *Environmental Research Letters*, *044018*. https://doi.org/10.1088/1748-9326/aa65a4

Sherwen, T., Schmidt, J. A., Evans, M. J., Carpenter, L. J., Großmann, K., Eastham, S. D., et al. (2016). Global impacts of tropospheric halogens (Cl, Br, I) on oxidants and composition in GEOS-Chem. *Atmospheric Chemistry and Physics*, *16*(18), 12239–12271. https://doi.org/10.5194/acp-16-12239-2016

Stettler, M. E. J., Eastham, S., & Barrett, S. R. H. (2011). Air quality and public health impacts of UK airports. Part I: Emissions. *Atmospheric Environment*, *45*(31), 5415–5424. https://doi.org/10.1016/j.atmosenv.2011.07.012

Tzompa-Sosa, Z. A., Mahieu, E., Franco, B., Keller, C. A., Turner, A. J., Helmig, D., et al. (2017). Revisiting global fossil fuel and biofuel emissions of ethane. *Journal of Geophysical Research: Atmospheres*, *122*(4), 2493–2512. https://doi.org/10.1002/2016JD025767

Van Der Werf, G. R., Randerson, J. T., Giglio, L., Collatz, G. J., Mu, M., Kasibhatla, P. S., et al. (2010). Global fire emissions and the contribution of deforestation, savanna, forest, agricultural, and peat fires (1997-2009). *Atmospheric Chemistry and Physics*, *10*(23), 11707–11735. https://doi.org/10.5194/acp-10-11707-2010

Vinken, G. C. M., Boersma, K. F., Jacob, D. J., & Meijer, E. W. (2011). Accounting for non-linear chemistry of ship plumes in the GEOS-Chem global chemistry transport model. *Atmospheric Chemistry and Physics*, *11*(22), 11707–11722. https://doi.org/10.5194/acp-11-11707-2011